Electronic Supplementary Material (ESI) for Inorganic Chemistry Frontiers.

Synthesis and Studies of Aqueous-Stable Diruthenium Aminocarbyne Complexes Uncovered an N-Indolyl Derivative as Prospective Anticancer Agent

Matteo Fiaschi,[a] Ján Vančo,[b] Lorenzo Biancalana,[a,*] Tomáš Malina,[b] Zdeněk Dvořák,[c] Tiziana Funaioli,[a] Stefano Zacchini,[d] Massimo Guelfi,[a] Zdeněk Trávníček,[b,*] and Fabio Marchetti[a,*]

[a] University of Pisa, Department of Chemistry and Industrial Chemistry, Via G. Moruzzi 13, I-56124 Pisa, Italy.

[b] Regional Centre of Advanced Technologies and Materials, Czech Advanced Technology and Research Institute, Palacký University, Šlechtitelů 27, CZ-779 00 Olomouc, Czech Republic.

[c] Department of Cell Biology and Genetics, Faculty of Science, Palacký University, Šlechtitelů 27, CZ-779 00 Olomouc, Czech Republic.

[d] University of Bologna, Department of Industrial Chemistry "Toso Montanari", Viale del Risorgimento 4, I-40136 Bologna, Italy.

Supporting Information

Table of contents — **Page(s)**

Synthesis and characterization of 1*H*-indol-5-yl isocyanide (5-isocyano-1*H*-indole)

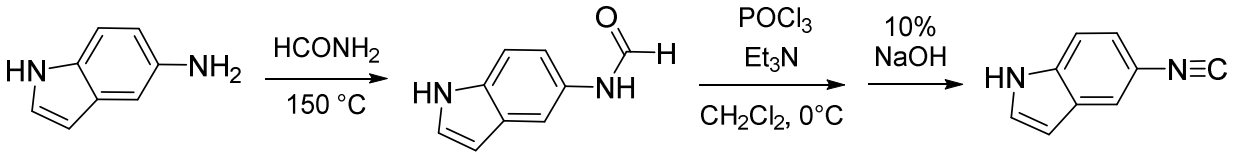

Scheme S1. Two-step synthesis of 1*H*-indol-5-yl isocyanide from 5-aminoindole.

The procedures reported below were modified with respect to the literature.[1,2]

***N*-(1*H*-indol-5-yl)formamide.**[1] A suspension of 5-aminoindole (1.245 g, 9.19 mmol) and formamide (6.2 mL, 156 mmol) was stirred at 150 °C overnight in a 10 mL Schlenk tube under N_2. The resulting dark red mixture was treated with water, ethyl acetate (*ca*. 20 mL each) and moved into a separatory funnel. The red-brown aqueous phase was discarded and the organic phase was extracted with water (x 2). Next, the organic phase was spiked with silica gel and volatiles were removed under vacuum. The solid was moved on top of a silica gel column (h 6.5 cm, d 4.3 cm). Impurities were eluted with CH_2Cl_2/acetone 4:1 *V*/*V* then a yellow band was eluted with CH_2Cl_2/acetone 2:1 *V*/*V* and taken to dryness under vacuum. The oily residue was treated with few mL of CH_2Cl_2 and taken to dryness again. The resulting faint yellow-pink (almost colorless) solid was dried under vacuum for several hours then moved into a 50-mL round bottom flask for the next step. Yield: 998 mg, 67.8 %.

Colorless solid. Soluble in acetone, poorly soluble in CH_2Cl_2, $CHCl_3$. ^{1}H NMR (acetone-d_6): δ/ppm = *10.28*, 10.20 (s-br, 1H); 9.05, *8.96* (s-br, 1H); *8.63* (d, *J* = 11.3 Hz), 8.34 (d, *J* = 1.6 Hz) (1H); 8.02 (s), *7.00* (dd, *J* = 8.7, 1.9 Hz) (1H); 7.45–7.28 (m, 3H), 6.49–6.41 (m, 1H). ^{13}C{^{1}H} NMR (acetone-d_6): δ/ppm = *163.3*, 159.4; 134.2; 131.7; 129.0; *127.0*, 126.5; *115.8*, 115.6; *112.9*, 112.0; 111.9, *111.5*; 102.4, *102.3*.

1*H*-indol-5-yl isocyanide, IndNC.[2] A suspension of *N*-(1*H*-indol-5-yl)formamide (998 mg, 6.23 mmol) and Et_3N (1.70 mL, 12.2 mmol) in anhydrous CH_2Cl_2 (15 mL) under nitrogen was cooled to 0

°C. $POCl_3$ (0.70 mL, 7.07 mmol) was added dropwise to the mixture under vigorous stirring at 0 °C. The resulting pale ochre-yellow solution was stirred for 2 h and allowed to slowly warm to room temperature. Next, the mixture was cooled to 0 °C and treated with a cold 10 % NaOH aqueous solution under vigorous stirring. The mixture was diluted with CH_2Cl_2, and the water phase was then moved into a separatory funnel. The aqueous phase was extracted with CH_2Cl_2 (3x) and the combined organic fractions were taken to dryness under vacuum. The residue was dissolved in a small volume of CH_2Cl_2 and filtered over celite. The filtrate was taken to dryness under vacuum and the residue was triturated in pentane (10 mL). The suspension was filtered and the resulting colorless (faint beige) solid was dried under vacuum (RT) and stored under N_2. Yield: 652 mg, 73.7 % (50 % overall yield from 5-aminoindole).

Colorless solid. Soluble in MeCN, CH_2Cl_2, poorly soluble in hexane, pentane. IR (CH_2Cl_2): $\tilde{\upsilon}/cm^{-1}$ = 2155w, 2127s (C≡N), 1607w-br, 1474m, 1457m, 1420m, 1347w, 1324m. IR (MeCN): $\tilde{\upsilon}/cm^{-1}$ = 2126s (C≡N). ^1H NMR ($CDCl_3$): δ/ppm = 8.39 (s-br, 1H, NH); 7.69 (s, 1H); 7.37 (d, *J* = 8.6 Hz, 1H); 7.31 (t, *J* = 2.8 Hz, 1H); 7.20 (d, *J* = 8.5 Hz, 1H); 6.60–6.57 (m, 1H). $^{13}C\{^1H\}$ NMR ($CDCl_3$): δ/ppm = 160.9 (CN); 135.3; 127.7; 126.6; 120.4; 119.3; 111.8; 103.3.

Recovery of unreacted [$Ru_2Cp_2(CO)_4$]

During the chromatographic purification of [**2a-g**]CF_3SO_3, yellow bands containing unreacted [$Ru_2Cp_2(CO)_4$] were eluted with CH_2Cl_2 and taken to dryness under vacuum. The following operations were carried out under N_2 using deaerated solvents (solutions of [$Ru_2Cp_2(CO)_4$] in CH_2Cl_2 slowly darkens when exposed to air).[3] The yellow-brown residue was suspended in hexane and moved on top of an alumina column. Impurities were eluted with hexane and hexane/Et_2O 1:1 *V*/*V*, then a yellow band was eluted with CH_2Cl_2. Volatiles were removed under vacuum, affording a yellow solid which was further dried under vacuum at 40 °C and stored under N_2.

IR characterization of $[Ru_2Cp_2(CO)_3(CNR)]$

Figure S1. Comparative view of IR spectra (1600-2200 cm^{-1}) of $[Ru_2Cp_2(CO)_4]$ (black line) and of the final reaction mixtures of $[Ru_2Cp_2(CO)_4]$ and MeNC (blue line), CyNC (red line), XylNC (dark green line; reaction time: 6 h) or IndNC (cyan line) in MeCN. Spectra are solvent-subtracted and normalized with respect to the transmittance of the bridging carbonyl stretching peak of $[Ru_2Cp_2(CO)_4]$ (1774 cm^{-1}).

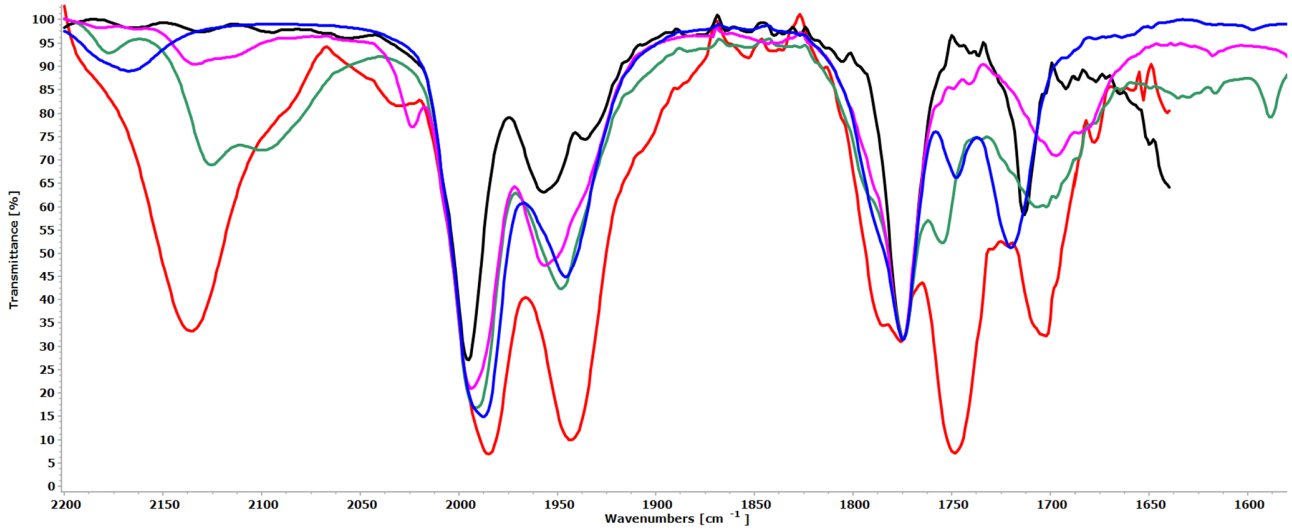

Figure S2. Comparative view of IR spectra (1600-2200 cm^{-1}) of $[Ru_2Cp_2(CO)_4]$ (black line) and of the final reaction mixtures of $[Ru_2Cp_2(CO)_4]$ and (2-naphthyl)NC (blue line), BnNC (red line), (*S*-PhCHMe)NC (dark green line) or (4-C_6H_4OMe)NC (cyan line) in THF. Spectra are solvent-subtracted and normalized with respect to the transmittance of the bridging carbonyl stretching peak of $[Ru_2Cp_2(CO)_4]$ (1782 cm^{-1}).

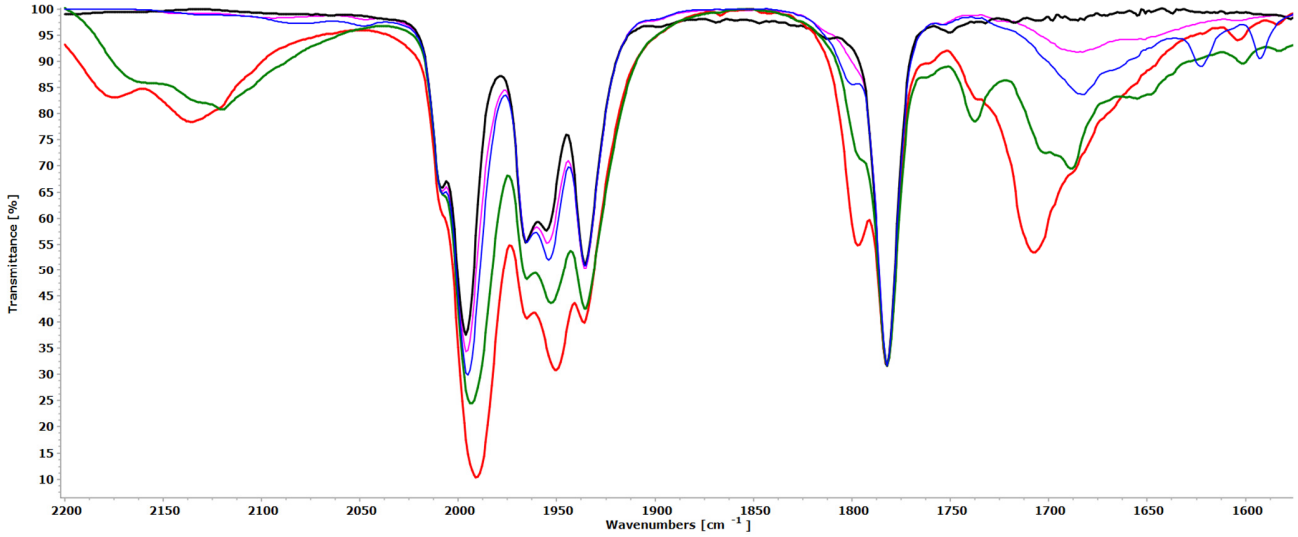

IR data for [$Ru_2Cp_2(CO)_3(CNR)$], 1a-h. Data refer to IR spectra of the reaction mixtures. Signals corresponding (or covered by) [$Ru_2Cp_2(CO)_4$] absorptions are marked with an asterisk (*). Terminal/bridging coordination is indicated as t/μ, respectively.

[$Ru_2Cp_2(CO)_3(CNMe)$], 1a. IR (MeCN): $\tilde{\upsilon}/cm^{-1}$ = 2068w (t-CN), 1988s (t-CO), 1946s (t-CO), 1787s-sh (μ-CO), 1775s* (μ-CO), 1748m (μ-CO), 1720m (μ-CN).

[$Ru_2Cp_2(CO)_3(CNCy)$], 1b. IR (MeCN): $\tilde{\upsilon}/cm^{-1}$ = 2136m (t-CN), 1985s (t-CO), 1943s (t-CO), 1786m (μ-CO), 1776m* (μ-CO), 1704m (μ-CN). IR (toluene): $\tilde{\upsilon}/cm^{-1}$ = 2133m (t-CN), 1995s (t-CO), 1965s* (t-CO), 1951s (t-CO), 1936s-sh* (t-CO), 1780s* (μ-CO), 1756s (μ-CO), 1706m (μ-CN).

[$Ru_2Cp_2(CO)_3(CNXyl)$], 1c. IR (MeCN): $\tilde{\upsilon}/cm^{-1}$ = 2127w (t-CN), 1991s* (t-CO), 1948m (t-CO), 1793w-sh (μ-CO), 1774m* (μ-CO), 1755m* (μ-CO), 1706w-br (μ-CN).

[$Ru_2Cp_2(CO)_3${CN(1*H*-indol-5-yl)}], 1d. IR (MeCN) $\tilde{\upsilon}/cm^{-1}$ = 2135w (t-CN ?), 1993s* (t-CO), 1790w-sh (μ-CO), 1775s (μ-CO), 1697m-br (μ-CN).

[$Ru_2Cp_2(CO)_3${CN(2-naphthyl)}], 1e. IR (THF): $\tilde{\upsilon}/cm^{-1}$ = 2130vw (t-CN ?), 1800m (μ-CO), 1683m (μ-CN). Other absorptions are covered by [$Ru_2Cp_2(CO)_4$].

[$Ru_2Cp_2(CO)_3${CN(4-C_6H_4OMe)}], 1f. IR (THF): $\tilde{\upsilon}/cm^{-1}$ = 2142vw (t-CN ?), 1686w (μ-CN). Other absorptions are covered by [$Ru_2Cp_2(CO)_4$].

[$Ru_2Cp_2(CO)_3(CNBn)$], 1g. IR (THF): $\tilde{\upsilon}/cm^{-1}$ = 2131w-br (t-CN), 1991s (t-CO), 1950s (t-CO), 1797m (μ-CO), 1707m-br (μ-CN).

IR and NMR characterization of $[Ru_2Cp_2(CO)_2(\mu\text{-}CO)\{\mu\text{-}CNMe(R)\}]CF_3SO_3$

Figure S3. Solid-state IR spectrum (650-4000 cm^{-1}) of $[Ru_2Cp_2(CO)_2(\mu\text{-}CO)\{\mu\text{-}CNMe_2\}]CF_3SO_3$, [**2a**]$CF_3SO_3$.

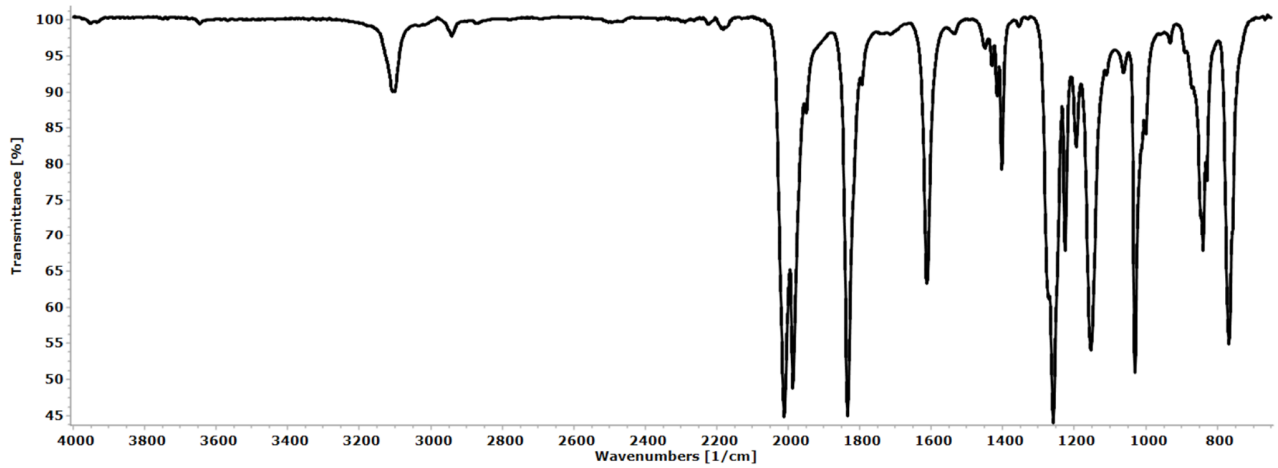

Figure S4. Comparison of IR spectra in CH_2Cl_2 (1500-2300 cm^{-1}) of [**2a**]CF_3SO_3 (blue line) and the diiron homologue [**2a**^{Fe}]CF_3SO_3 (red line). Transmittance of bridging carbonyl stretching peak (*ca*. 1840 cm^{-1}) is normalized.

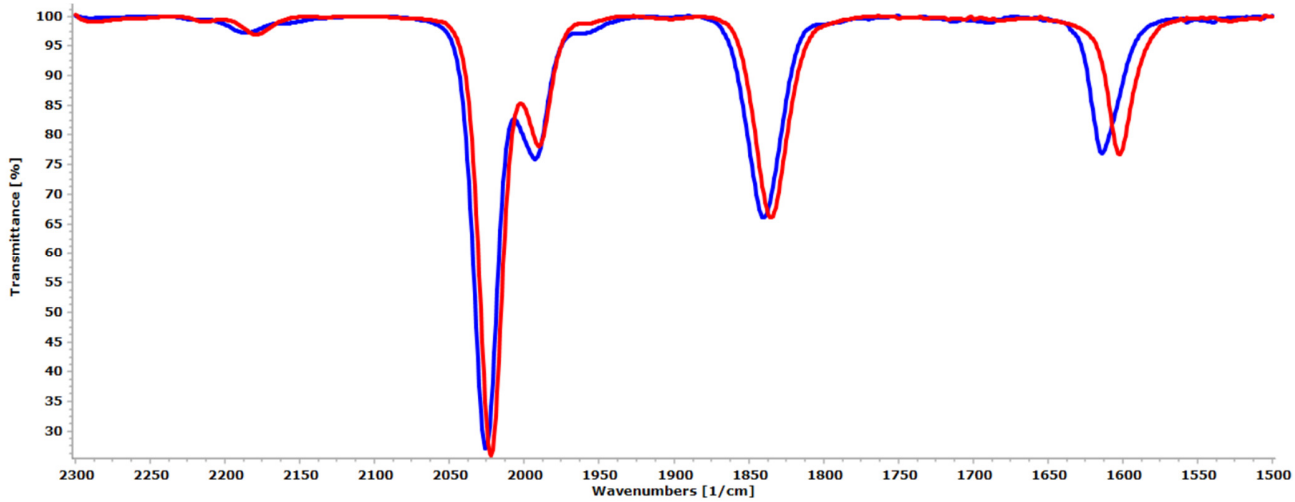

Figure S5. Solid-state IR spectrum (650-4000 cm^{-1}) of $[Ru_2Cp_2(CO)_2(\mu\text{-}CO)\{\mu\text{-}CNMe(Cy)\}]CF_3SO_3$, [**2b**]$CF_3SO_3$.

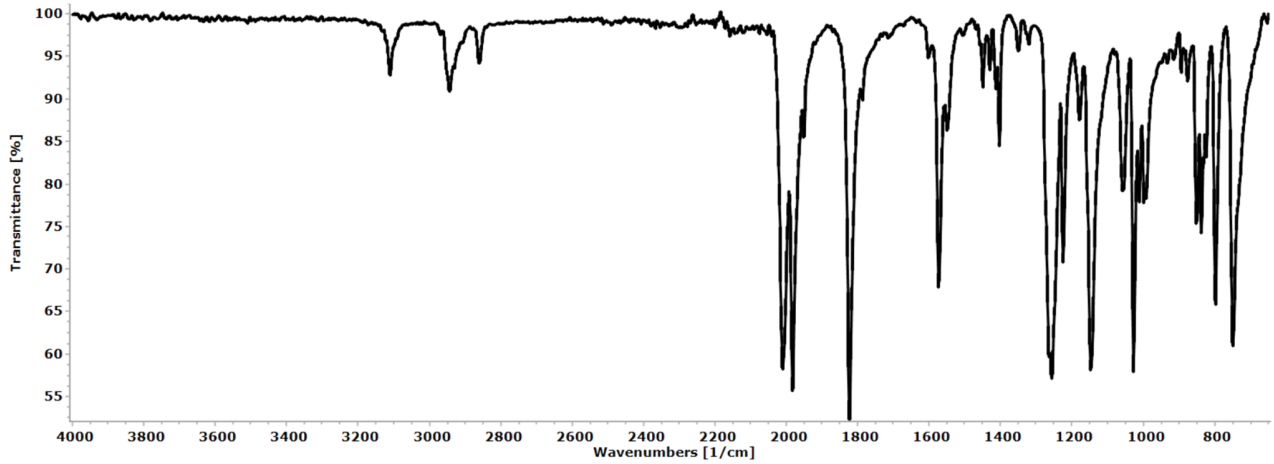

Figure S6. Comparison of IR spectra in CH_2Cl_2 (1500-2300 cm^{-1}) of [**2b**]CF_3SO_3 (blue line) and the diiron homologue [**2b^{Fe}**]CF_3SO_3 (red line). Transmittance of bridging carbonyl stretching peak (*ca*. 1840 cm^{-1}) is normalized.

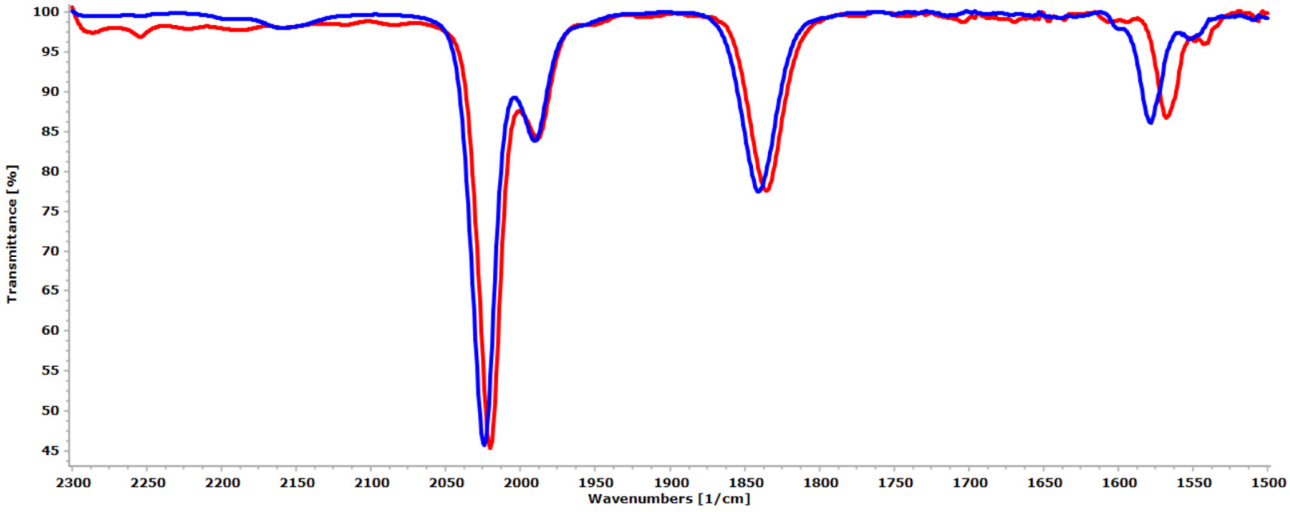

Figure S7. Solid-state IR spectrum (650-4000 cm^{-1}) of $[Ru_2Cp_2(CO)_2(\mu\text{-}CO)\{\mu\text{-}CNMe(Xyl)\}]CF_3SO_3$, [**2c**]$CF_3SO_3$.

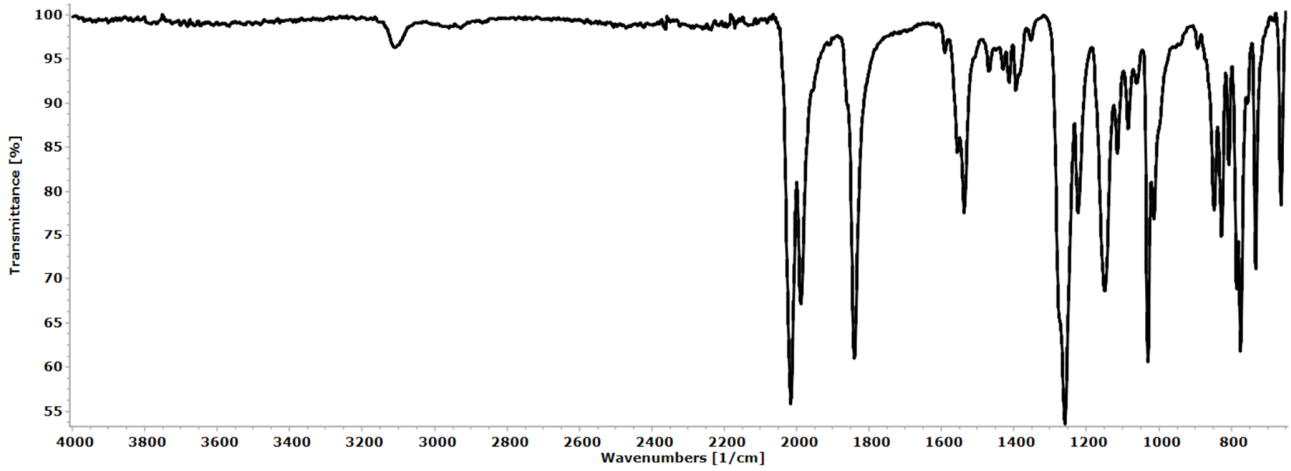

Figure S8. Comparison of IR spectra in CH_2Cl_2 (1500-2300 cm^{-1}) of [**2c**]CF_3SO_3 (blue line) and the diiron homologue [**2c**^{Fe}]CF_3SO_3 (red line). Transmittance of bridging carbonyl stretching peak (*ca*. 1840 cm^{-1}) is normalized.

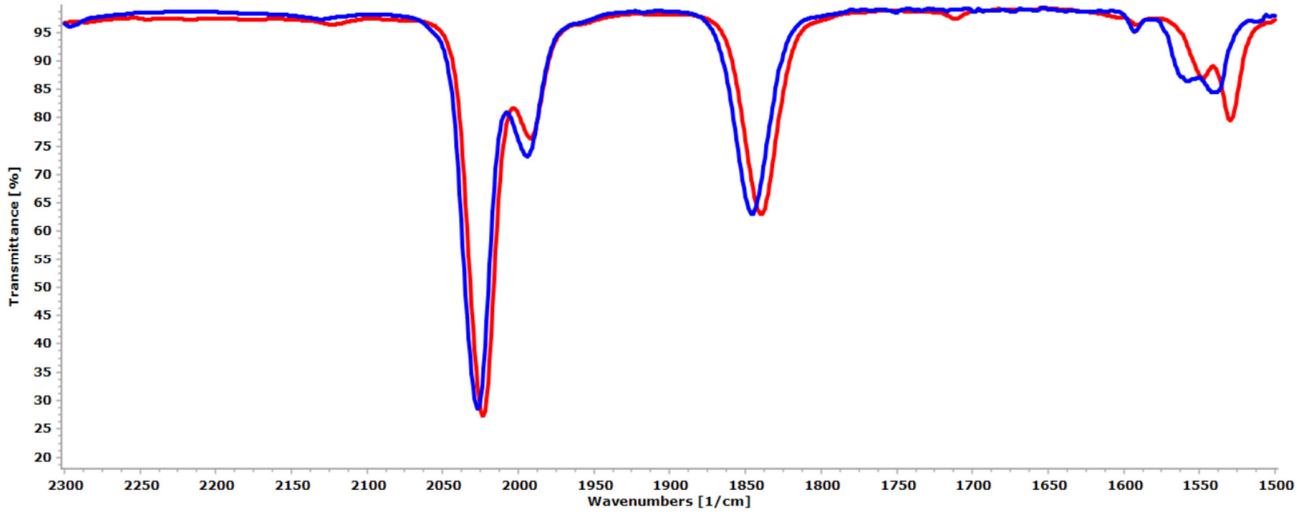

Figure S9. Solid-state IR spectrum (650-4000 cm^{-1}) of $[Ru_2Cp_2(CO)_2(\mu\text{-}CO)\{\mu\text{-}CNMe(1H\text{-}indol\text{-}5\text{-}yl)\}]CF_3SO_3$, [**2d**]$CF_3SO_3$.

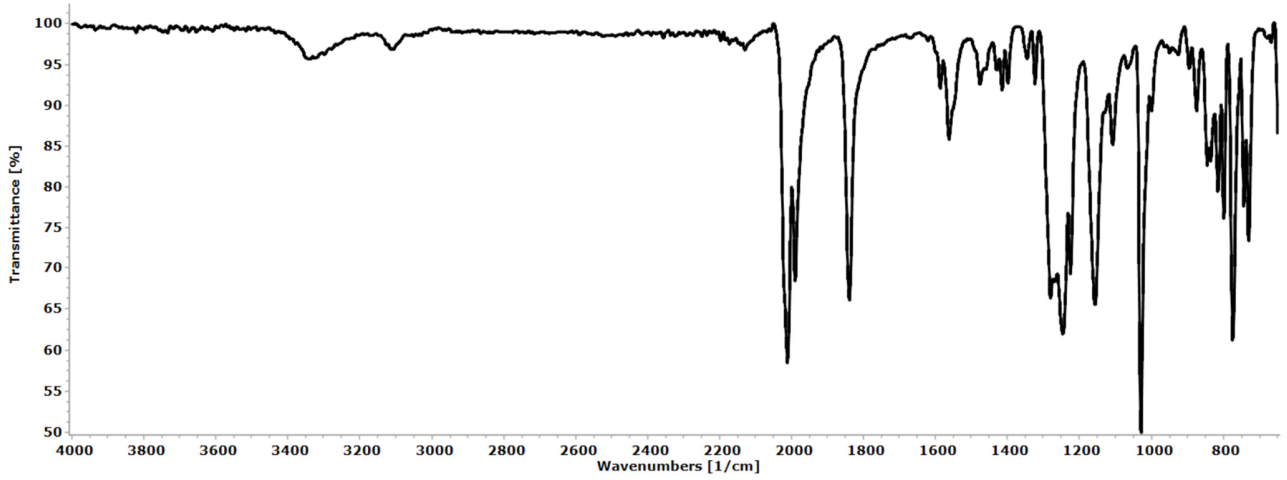

Figure S10. Comparison of IR spectra in CH_2Cl_2 (1500-2300 cm^{-1}) of [**2d**]CF_3SO_3 (blue line) and the diiron homologue [$\mathbf{2d^{Fe}}$]CF_3SO_3 (red line). Transmittance of bridging carbonyl stretching peak (*ca*. 1840 cm^{-1}) is normalized.

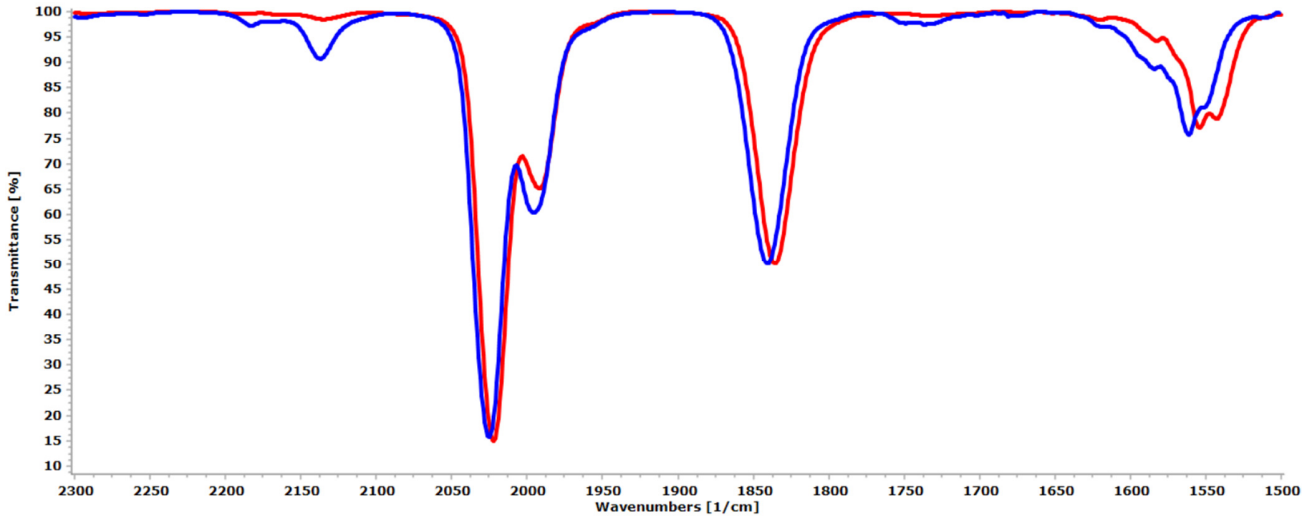

Figure S11. Comparison of IR spectra in CH_2Cl_2 (1500-2300 cm^{-1}) of $[Ru_2Cp_2(CO)_2(\mu\text{-}CO)\{\mu\text{-}CNMe(2\text{-}naphthyl)\}]CF_3SO_3$, [**2e**]$CF_3SO_3$ (blue line) and the diiron homologue [**2e**^{Fe}]CF_3SO_3 (red line). Transmittance of bridging carbonyl stretching peak (*ca*. 1840 cm^{-1}) is normalized.

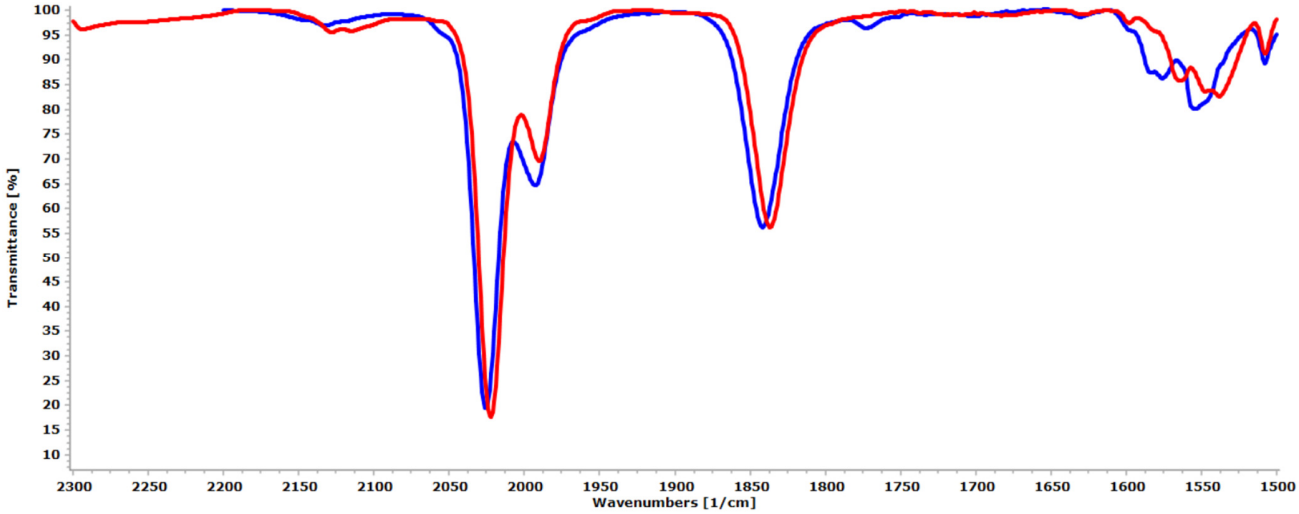

Figure S12. ^{1}H NMR spectrum (401 MHz, acetone-d_6) of $[Ru_2Cp_2(CO)_2(\mu\text{-}CO)\{\mu\text{-}CNMe_2\}]CF_3SO_3$, [**2a**]$CF_3SO_3$. The integration is related to the signals of the major (*cis*) + minor (*trans*) isomers.

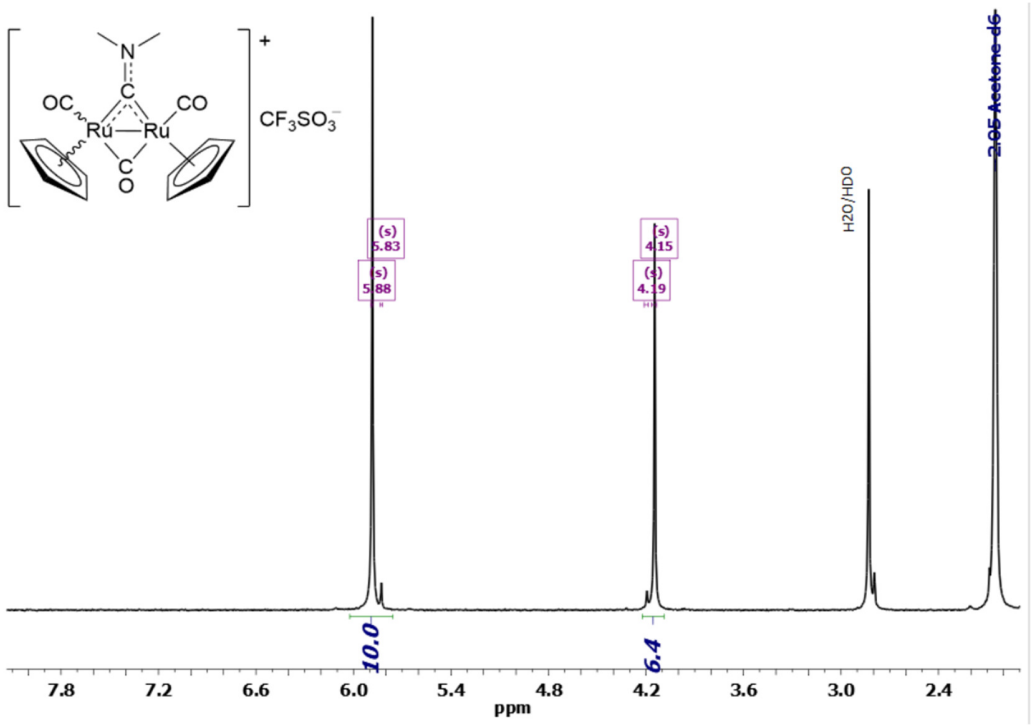

Figure S13. $^{13}C\{^{1}H\}$ NMR spectrum (101 MHz, acetone-d_6) of [**2a**]CF_3SO_3.

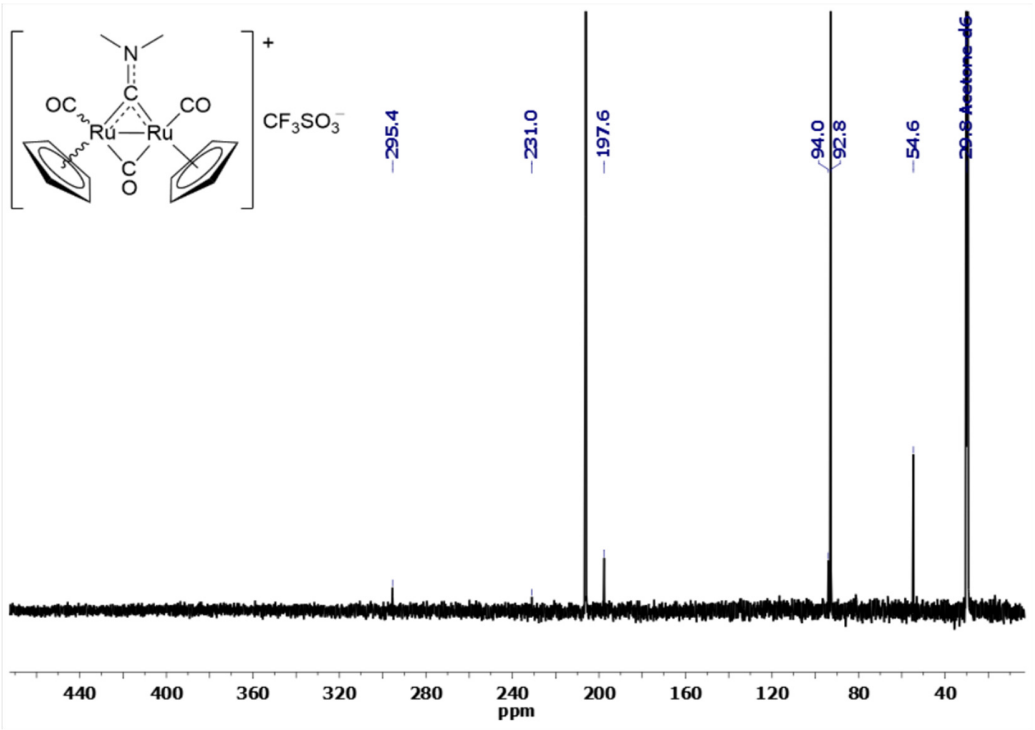

Figure S14. ^{1}H NMR spectrum (401 MHz, $CDCl_3$) of $[Ru_2Cp_2(CO)_2(\mu\text{-}CO)\{\mu\text{-}CNMe(Cy)\}]CF_3SO_3$, [**2b**]$CF_3SO_3$. The integration is related to the signals of the major (*cis*) + minor (*trans*) isomers.

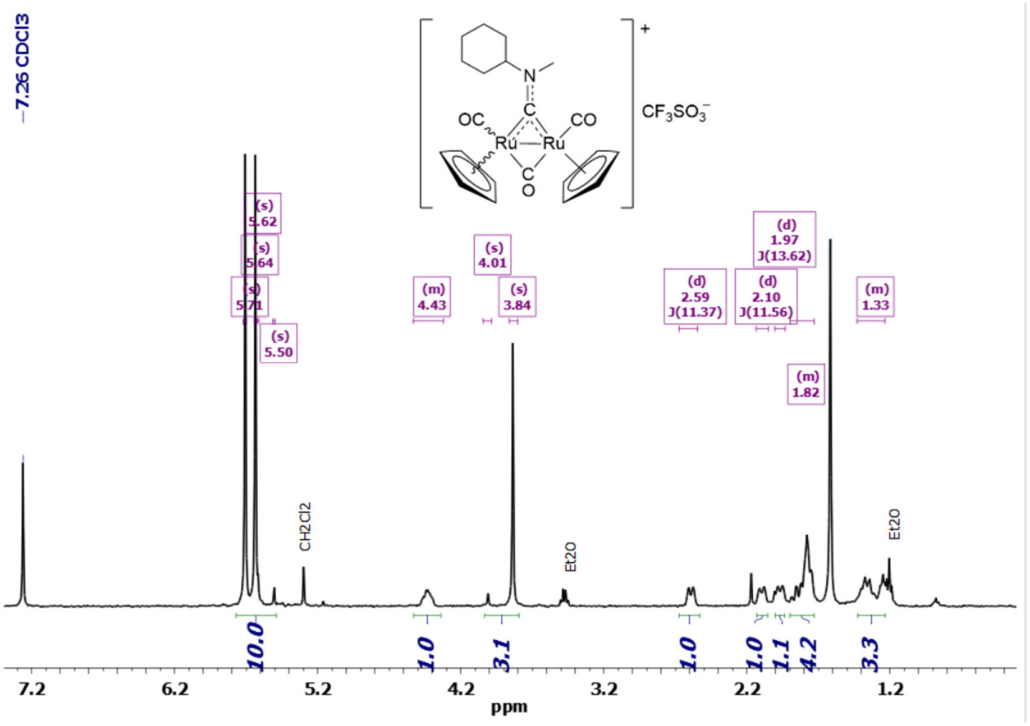

Figure S15. $^{13}C\{^{1}H\}$ NMR spectrum (101 MHz, $CDCl_3$) of [**2b**]CF_3SO_3.

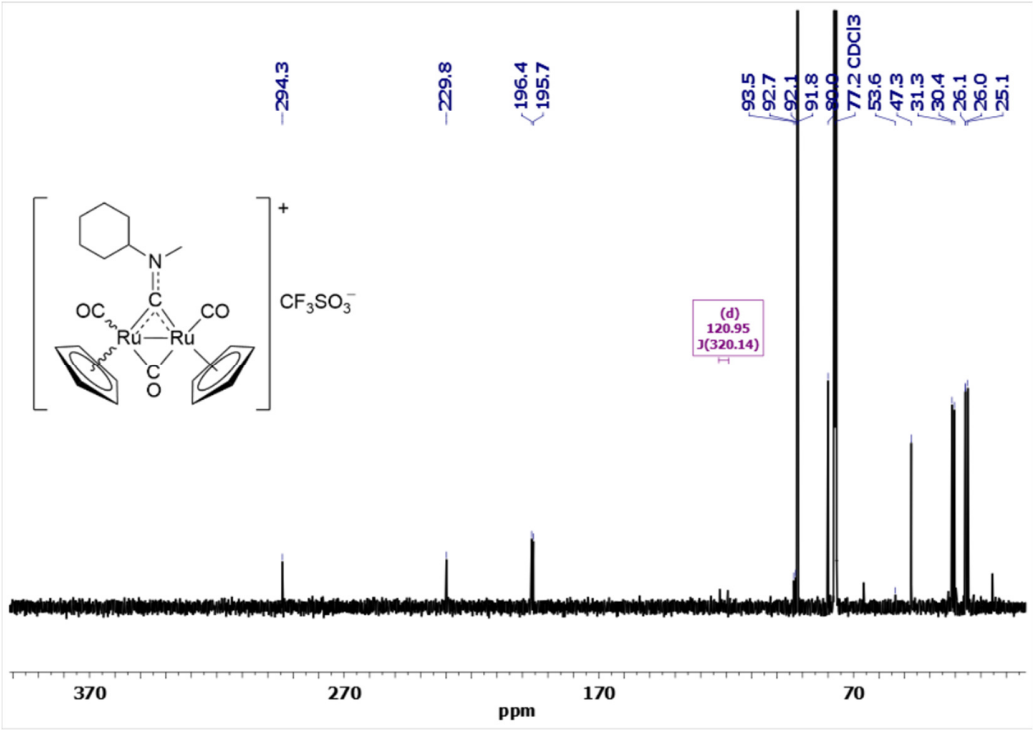

Figure S16. Black line: ^{1}H NMR spectrum (401 MHz, acetone-d_6) of *cis*-[**2b**]CF_3SO_3. Blue line: ^{1}H NOESY with irradiation at 5.71 ppm (Cp). Red line: ^{1}H NOESY with irradiation at 5.64 ppm (Cp'). Observed NOEs are indicated by the arrows. The NOE effect between Cp and Cp' is weakened by co-irradiation (dotted blue line).

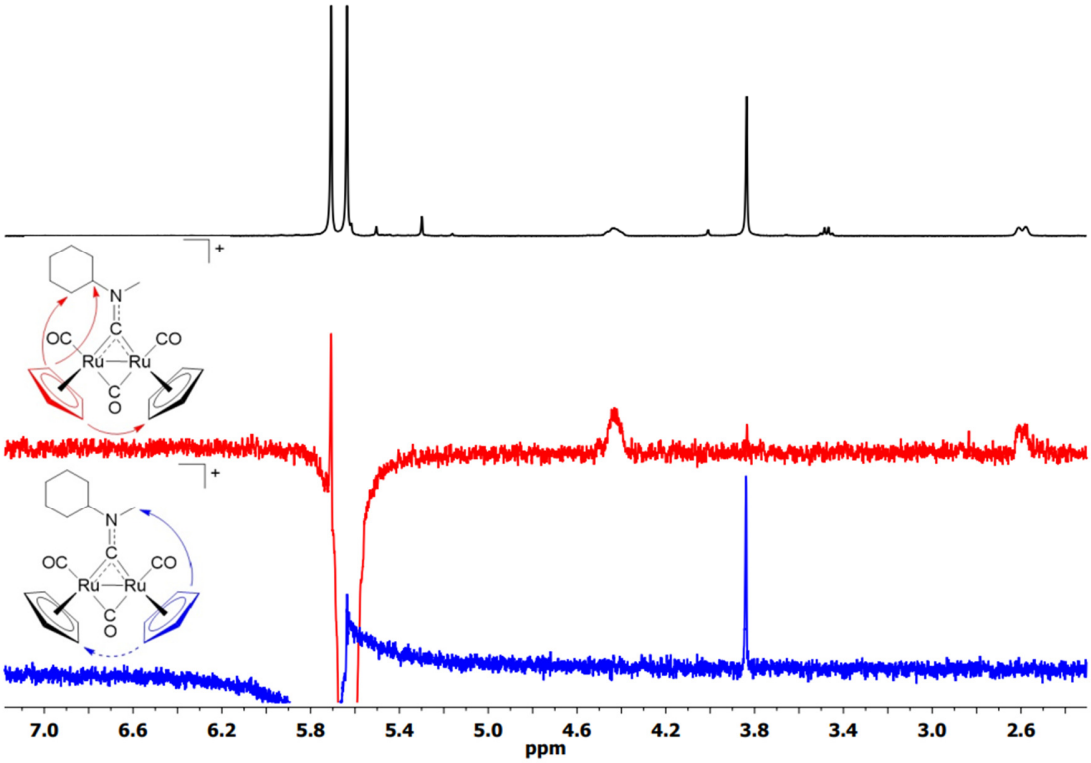

Figure S17. ^{1}H NMR spectrum (401 MHz, $CDCl_3$) of $[Ru_2Cp_2(CO)_2(\mu\text{-}CO)\{\mu\text{-}CNMe(Xyl)\}]CF_3SO_3$, [**2c**]$CF_3SO_3$.

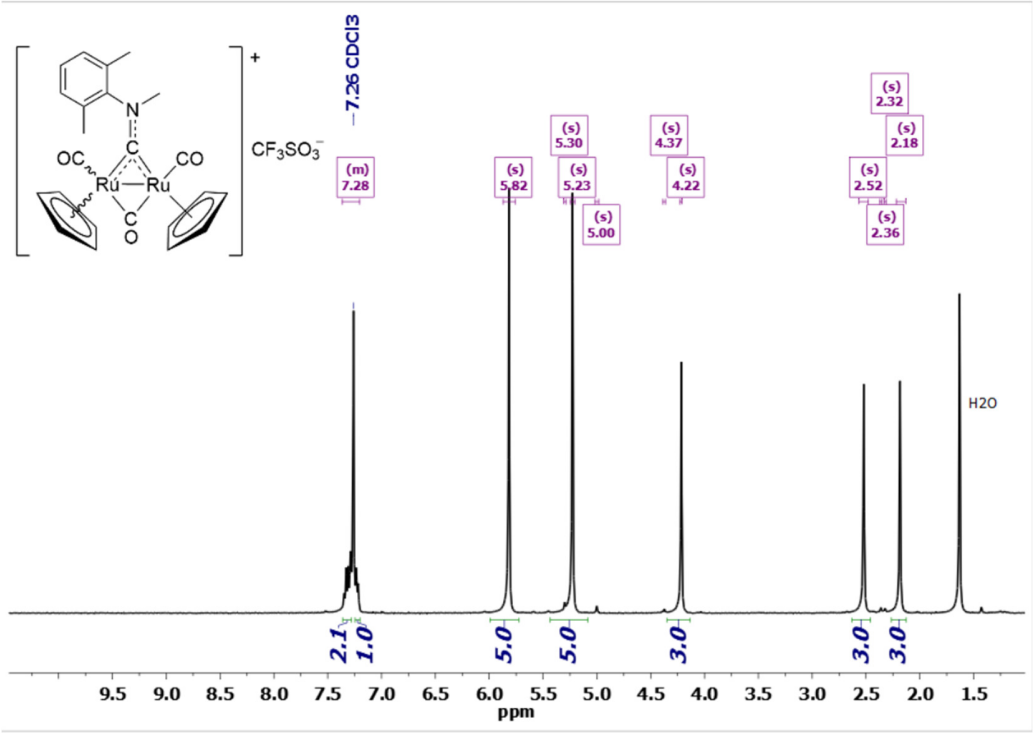

Figure S18. $^{13}C\{^{1}H\}$ NMR spectrum (101 MHz, $CDCl_3$) of [**2c**]CF_3SO_3.

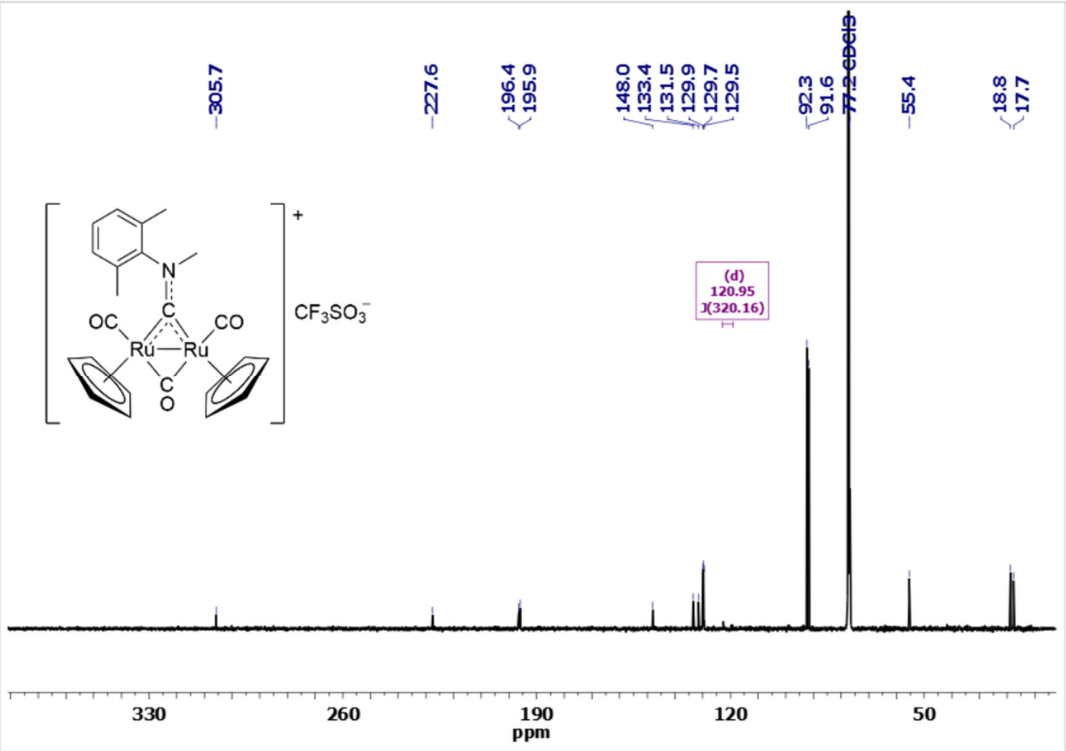

Figure S19. Black line: ^{1}H NMR spectrum (401 MHz, acetone-d_6) of *cis*-[**2c**]CF_3SO_3. Blue line: ^{1}H NOESY with irradiation at 5.82 ppm (Cp). Red line: ^{1}H NOESY with irradiation at 5.23 ppm (Cp'). Observed NOEs are indicated by the arrows.

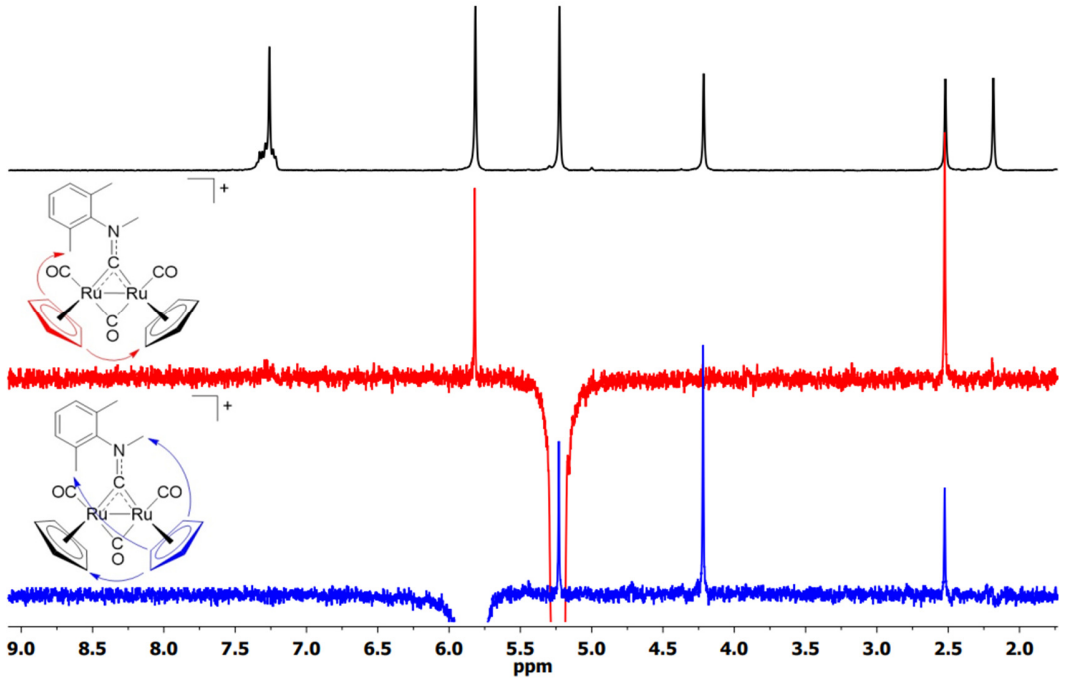

Figure S20. ^{1}H NMR spectrum (401 MHz, acetone-d_6) of $[Ru_2Cp_2(CO)_2(\mu\text{-}CO)\{\mu\text{-}CNMe(1H\text{-indol-5-yl})\}]CF_3SO_3$, [**2d**]$CF_3SO_3$. The integration is related to the signals of the major (*cis*) + minor (*trans*) isomers.

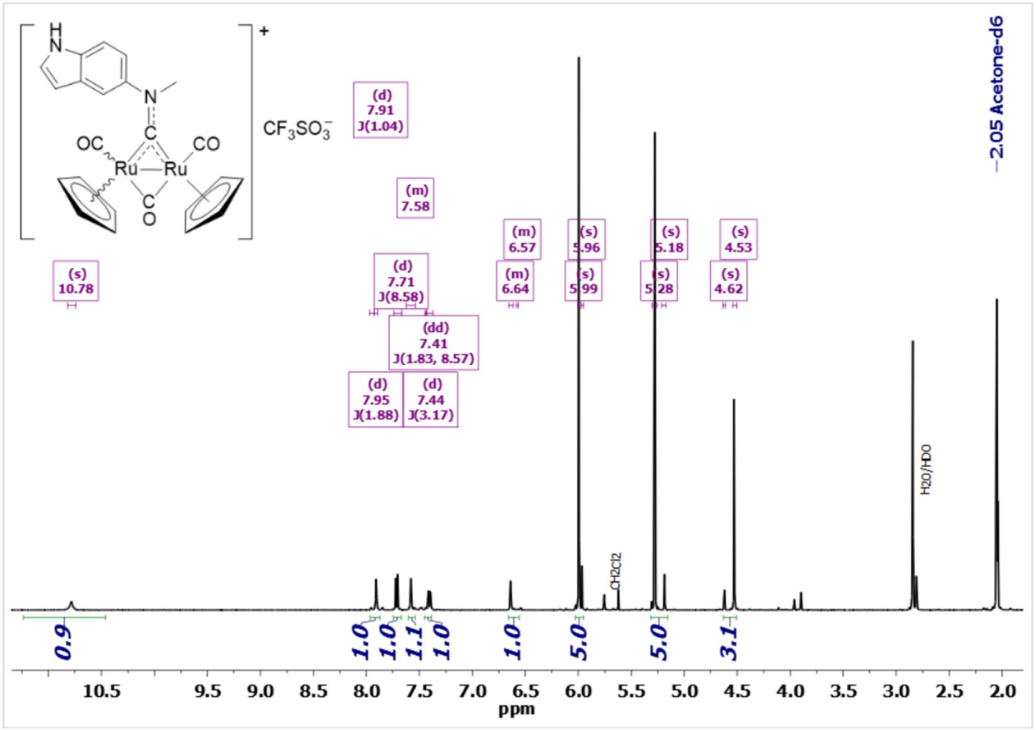

Figure S21. $^{13}C\{^{1}H\}$ NMR spectrum (101 MHz, acetone-d_6) of [**2d**]CF_3SO_3.

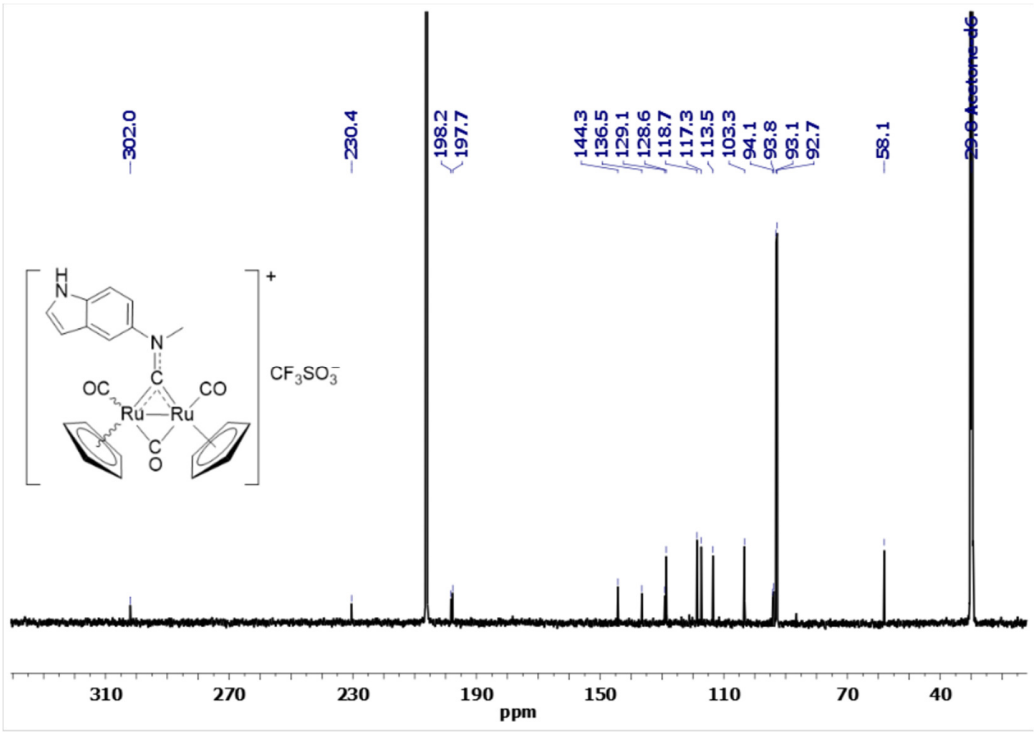

Figure S22. Black line: ^{1}H NMR spectrum (401 MHz, acetone-d_6) of *cis*-[**2d**]CF_3SO_3. Blue line: ^{1}H NOESY with irradiation at 5.99 ppm (Cp). Red line: ^{1}H NOESY with irradiation at 5.28 ppm (Cp'). Observed NOEs are indicated by the arrows.

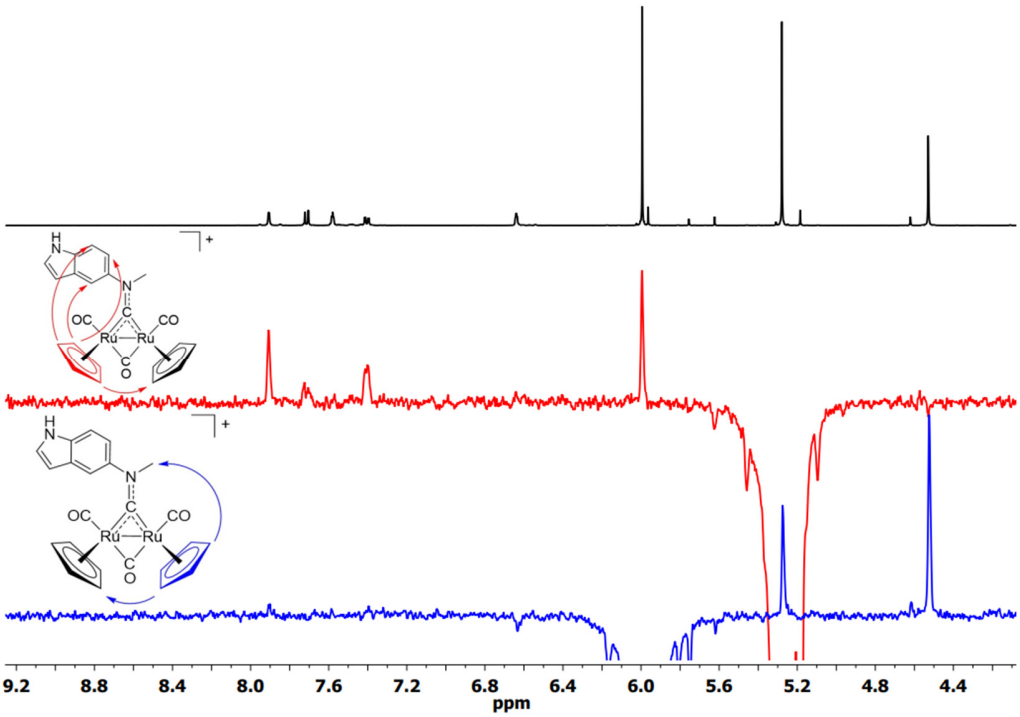

Figure S23. ^{1}H NMR spectrum (401 MHz, $CDCl_3$) of $[Ru_2Cp_2(CO)_2(\mu\text{-}CO)\{\mu\text{-}CNMe(2\text{-naphthyl})\}]CF_3SO_3$, [**2e**]$CF_3SO_3$. The integration is related to the signals of the major (*cis*) + minor (*trans*) isomers.

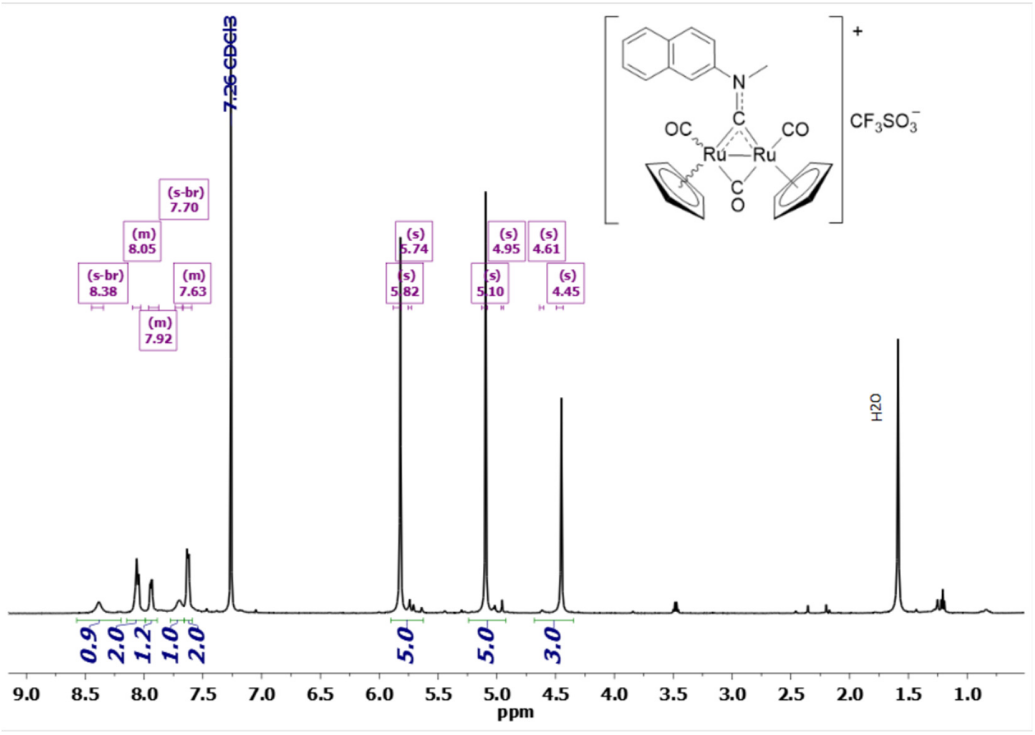

Figure S24. ^{1}H NMR spectrum (401 MHz, $CDCl_3$) of $[Ru_2Cp_2(CO)_2(\mu\text{-}CO)\{\mu\text{-}CNMe(4\text{-}C_6H_4OMe)\}]CF_3SO_3$, [**2f**]$CF_3SO_3$ + impurities. Only the signals of the major isomer are highlighted and integrated.

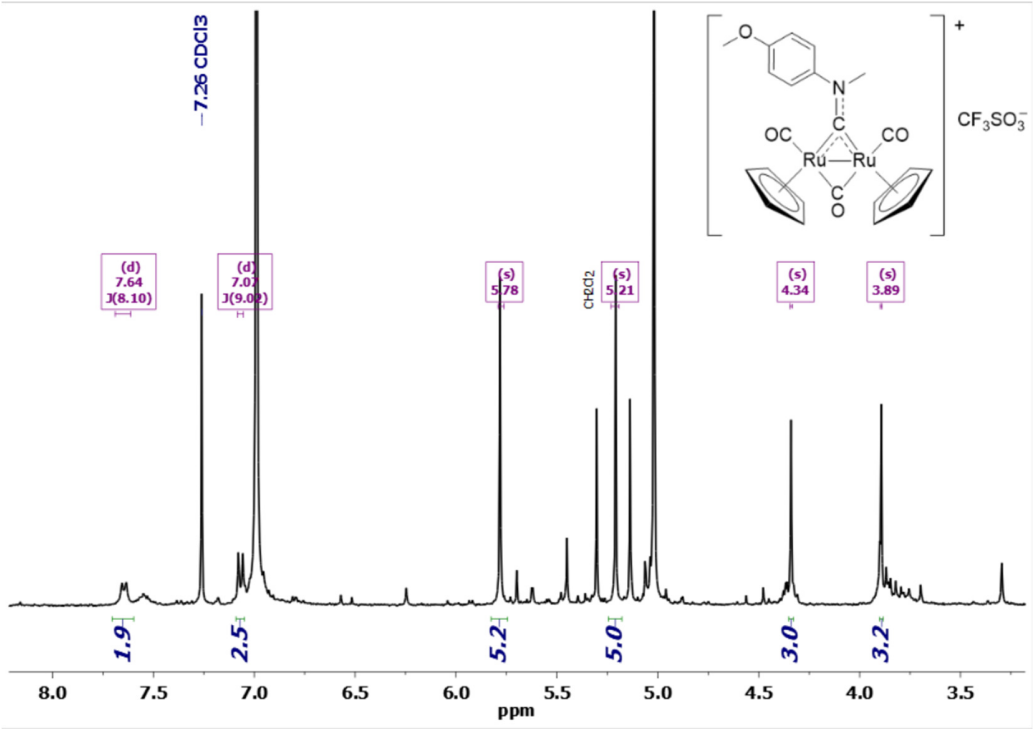

Figure S25. ^{1}H NMR spectrum (401 MHz, $CDCl_3$) of $[Ru_2Cp_2(CO)_2(\mu\text{-}CO)\{\mu\text{-}(S)\text{-}CN(Me)CH(Me)Ph)\}]CF_3SO_3$, [**2g**]$CF_3SO_3$ + impurities. Only the signals of the major isomer are highlighted and integrated.

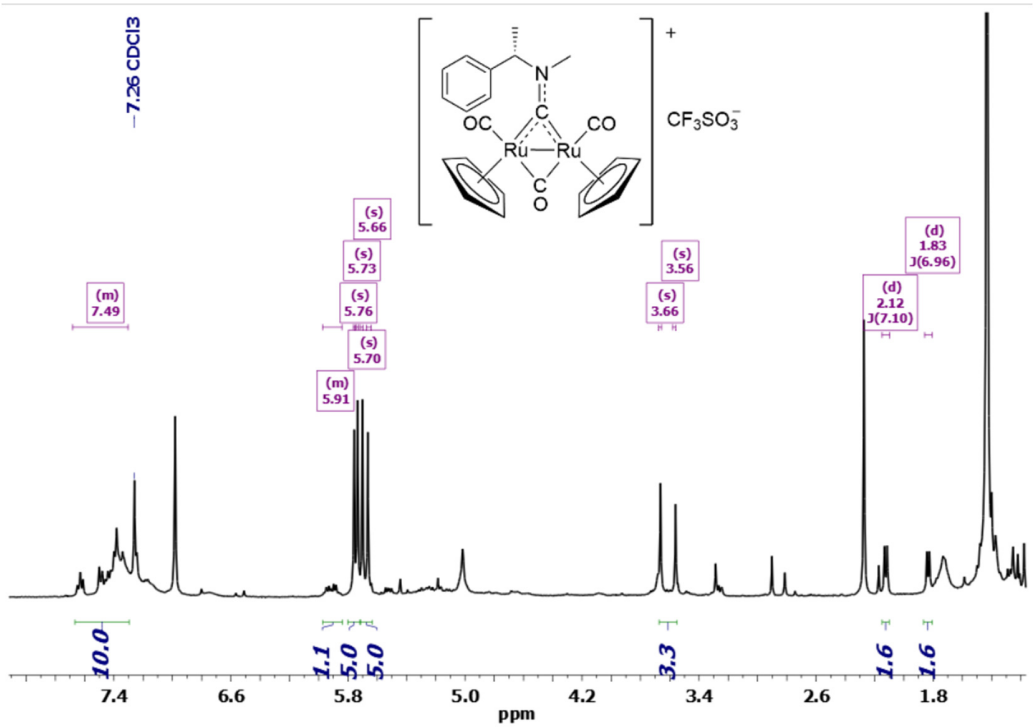

Table S1. Comparison of selected IR data for *cis*-[$M_2Cp_2(CO)_2$(μ-CO){μ-CNMe(R)}]$^+$ (M = Fe, Ru) complexes.

R [c]	Complex [a]	IR (CH_2Cl_2): ũ / cm^{-1}				IR (solid state): ũ / cm^{-1}			
		v(t-CO)	v(t-CO)	v(μ-CO)	v(μ-CN)	v(t-CO)	v(t-CO)	v(μ-CO)	v(μ-CN)
Me	[**2a**]$^+$	2026	1993	1840	1614	2011	1987	1834	1612
	[**2a^{Fe}**]$^+$ [b]	2022	1990	1835	1602	2021	1991	1814	1592
	Δ (Fe→Ru)	*+4*	*+3*	*+5*	*+12*	*-10*	*-4*	*+ 20*	*+ 20*
Cy	[**2b**]$^+$	2024	1990	1841	1578	2010	1983	1823	1573
	[**2b^{Fe}**]$^+$ [b]	2020	1988	1835	1567	2006	1982	1822	1565
	Δ (Fe→Ru)	*+4*	*+2*	*+6*	*+11*	*+4*	*+1*	*+1*	*+8*
Xyl	[**2c**]$^+$	2027	1994	1846	1540	2017	1988	1841	1538
	[**2c^{Fe}**]$^+$ [b]	2023	1992	1840	1530	2012	1989	1832	1527
	Δ (Fe→Ru)	*+4*	*+2*	*+6*	*+10*	*+5*	*-1*	*+9*	*+11*
Ind	[**2d**]$^+$	2025	1995	1841	1548	2011	1990	1840	1548
	[**2d^{Fe}**]$^+$ [b]	2022	1992	1836	1542	2004	1985	1833	1540
	Δ (Fe→Ru)	*+3*	*+3*	*+5*	*+6*	*+7*	*+5*	*+7*	*+8*
Naph	[**2e**]$^+$	2026	1993	1842	1544	*n.r.*			
	[**2e^{Fe}**]$^+$ [b]	2022	1990	1837	1538				
	Δ (Fe→Ru)	*+4*	*+3*	*+ 5*	*+ 6*				
*p*Anis	[**2f**]$^+$	2025	1991	1841	1550	*n.r.*			
	[**2f^{Fe}**]$^+$ [b]	2021	1989	1836	1540				
	Δ (Fe→Ru)	*+4*	*+2*	*+5*	*+10*				
Bn	[**2h**]$^+$ [b]	2025	1992	1841	1582	*n.r.*			
	[**2h^{Fe}**]$^+$ [b]	2020	1898	1836	1576				
	Δ (Fe→Ru)	*+5*	*+3*	*+5*	*+6*				

[a] All complexes as $CF_3SO_3^-$ salts. [b] Diiron homologue of the respective diruthenium complex. Data taken from the literature.[Errore. Il segnalibro non è definito.,4,5,6] [c] Abbreviation list: Cy = C_6H_{11}, Xyl = 2,6-$C_6H_3Me_2$, Ind = 1*H*-indol-5-yl, Naph = 2-naphthyl, *p*Anis = 4-C_6H_4OMe, Bn = CH_2Ph. *n.r.* = not recorded.

$[Fe_2Cp_2(CO)_2(\mu\text{-}CO)\{\mu\text{-}CNMe(Xyl)\}]CF_3SO_3$, [**2c^{Fe}**]$CF_3SO_3$.[6] The IR spectrum was recorded for comparative purposes. IR (solid state): ũ/cm^{-1} = 3112w, 2012s (CO), 1989s-sh (CO), 1832s (μ-CO), 1590w, 1546m-sh, 1527m (μ-CN), 1505w-sh, 1469w, 1434w, 1420w, 1393m, 1384w-sh, 1362w, 1272s-sh, 1259s (SO_3), 1223m-sh (SO_3), 1212m-sh, 1151s (SO_3), 1114m, 1085m, 1067w, 1030s, 1009m-sh, 859m, 840m, 807w, 786m, 770s, 732s, 665s.

Table S2. Comparison of selected NMR data for *cis*-[$M_2Cp_2(CO)_2$(μ-CO){μ-CNMe(R)}]$^+$ (M = Fe, Ru) complexes.

R [a]	Complex [b]	^{13}C NMR [c]: δ / ppm						^{1}H NMR [c]: δ / ppm		
		μ-CN	μ-CO	t-CO	Cp	Cp'	NCH_3	Cp	Cp'	NMe
Me	[**2a**]$^+$	295.4	231.0	197.6	92.8		54.6	5.88		4.15
	[**2a^{Fe}**]$^+$ [d]	315.5	257.6	209.3	90.8		54.6	5.54		4.35
	Δ (Fe→Ru)	*- 20.1*	*- 26.6*	*- 11.7*	*+2*		*0*	*+ 0.34*		*- 0.20*
Cy	[**2b**]$^+$	294.3	229.8	196.4, 195.7	92.1	91.8	47.3	5.71	5.64	3.84
	[**2b^{Fe}**]$^+$ [d]	316.4	255.3	208.5, 207.6	90.3	90.1	46.8	5.36	5.27	4.06
	Δ (Fe→Ru)	*- 22.1*	*- 25.5*	*- 12.1, - 11.9*	*+1.8*	*+1.7*	*0.5*	*+ 0.35*	*+ 0.37*	*- 0.22*
Xyl	[**2c**]$^+$	305.7	227.6	196.4, 195.9	92.3	91.6	55.4	5.82	5.23	4.21
	[**2c^{Fe}**]$^+$ [d]	327.8	253.9	208.6	91.3	91.1	56.3	5.48	4.83	4.44
	Δ (Fe→Ru)	*- 22.1*	*- 26.3*	*- 12.2, - 12.7*	*+1.0*	*+0.5*	*- 0.9*	*+ 0.34*	*+ 0.40*	*- 0.23*
Ind	[**2d**]$^+$	302.0	230.4	198.3, 197.7	93.1	92.7	58.1	5.99	5.28	4.53
	[**2d^{Fe}**]$^+$ [d]	324.9	255.9	209.8, 209.2	91.2	91.0	58.5	5.39	4.65	4.53
	Δ (Fe→Ru)	*- 22.9*	*- 25.5*	*- 11.5, - 11.5*	*+1.9*	*+1.7*	*- 0.4*	*+ 0.60*	*+ 0.63*	*0*

[a] Abbreviation list: Cy = C_6H_{11}, Xyl = 2,6-$C_6H_3Me_2$, Ind = 1*H*-indol-5-yl. [b] All complexes as $CF_3SO_3^-$ salts. [c] NMR data in $CDCl_3$ except [**2a**]$^+$ (acetone-d_6), [**2a^{Fe}**]$^+$ (^{1}H: acetone-d_6, ^{13}C: DMSO-d_6), [**2d**]$^+$ (acetone-d_6), [**2d^{Fe}**]$^+$ (CD_3CN). [d] Diiron homologue of the respective diruthenium complex. Data taken from the literature.[4,6]

Synthesis and characterization of [3a]CF_3SO_3

Chart S1. Structure of $[Ru_2Cp_2(CO)(NCMe)(\mu\text{-}CO)\{\mu\text{-}CNMe_2\}]^+$, [**3a**]$^+$.

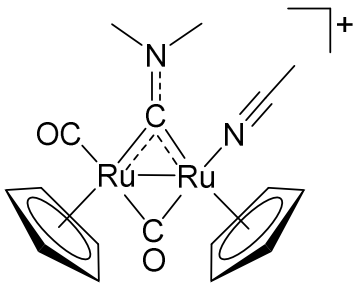

The title compound was prepared according to a modified literature procedure.[7] A solution of [**2a**]CF_3SO_3 in deaerated MeCN (10 mL) under N_2 was treated with $Me_3NO{\cdot}2H_2O$ (75 mg, 0.67 mmol) and stirred at room temperature for 1 h. Conversion was checked by IR then volatiles were removed under vacuum. The brown residue was dissolved in CH_2Cl_2 and moved on top of an alumina column (h 4, d 3.4 cm). Impurities were eluted with CH_2Cl_2 then a brown band was collected with MeCN and taken to dryness under vacuum. The residue was triturated in Et_2O and the suspension was filtered. The resulting brown solid was washed with Et_2O and dried under vacuum (40 °C). Yield: 124 mg, 61 %. Alternatively, [**3a**]$^+$ formed during alumina chromatography of [**2a**]$^+$ using MeCN as eluent, and a mixture of the two $CF_3SO_3^-$ salts was obtained upon volatiles removal under vacuum. Anal. calcd. for $C_{18}H_{19}F_3N_2O_5Ru_2S$: C, 34.07; H, 3.02; N, 4.41; S, 5.05. Found: C, 33.8; H, 2.98; N, 4.36; S, 5.00. IR (solid state): $\tilde{\upsilon}/cm^{-1}$ = 3116-3087w, 2986w, 2940w, 2930w, 2221w-br (C≡N), 2191w, 2175w, 1973s (CO), 1789s (μ-CO), 1608m (μ-CN), 1557w-sh, 1430w, 1412w, 1398m, 1354w, 1277s-sh, 1259s (SO_3), 1224m-sh (SO_3), 1201m, 1145s (SO_3), 1062w, 1029s, 1014m-sh, 996m-sh, 875w, 840m, 817m, 779s, 753m-sh. IR (CH_2Cl_2): $\tilde{\upsilon}/cm^{-1}$ = 1981s (CO), 1814s (μ-CO), 1595m (μ-CN), 1559w. ^{1}H NMR (acetone-d_6): δ/ppm = 5.60 (s, 5H, Cp); 5.37 (s, 5H, Cp'); 4.18 (s, 3H, NCH_3); 4.08 (s, 3H, NCH_3'); 2.27 (s, 3H, CCH_3); signals ascribable to a second (*trans*) isomer were not detected.

Figure S26. ^{1}H NMR spectrum (401 MHz, acetone-d_6) of $[Ru_2Cp_2(CO)(NCMe)(\mu\text{-}CO)\{\mu\text{-}CNMe_2\}]CF_3SO_3$, [**3a**]$CF_3SO_3$.

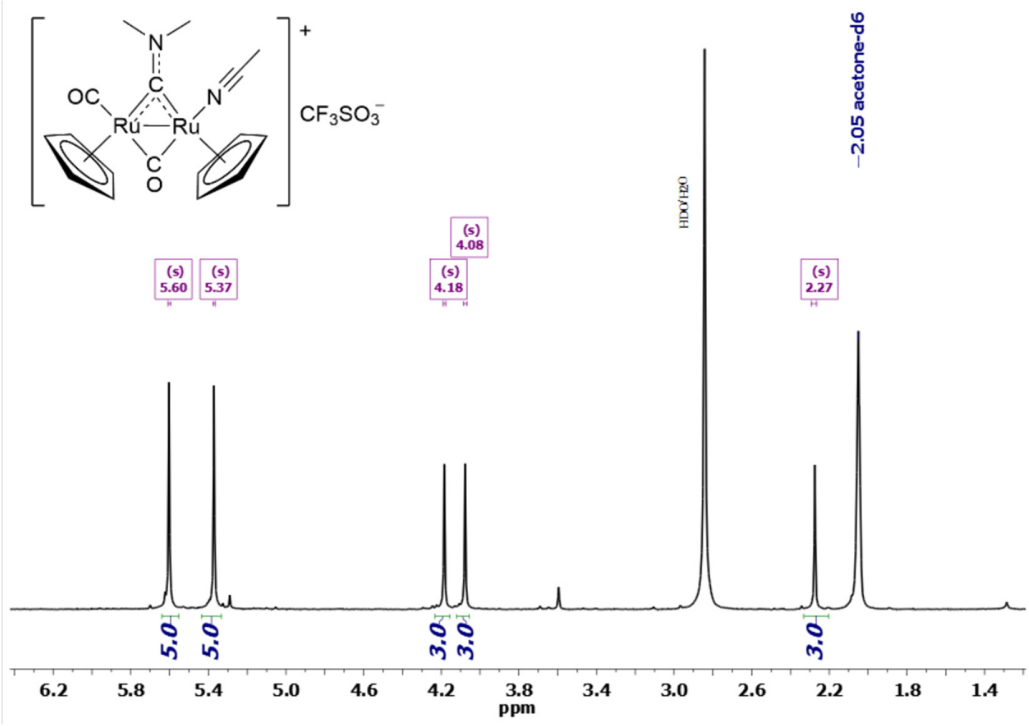

Log P_{ow}, solubility and stability studies in aqueous media

Table S3. Comparison of solubility in water (D_2O) and octanol-water partition coefficient (Log_{10} P_{ow}) for $[M_2Cp_2(CO)_2(\mu\text{-}CO)\{\mu\text{-}CNMe(R)\}]^+$ (M = Fe, Ru) complexes.

Complex [a]	D_2O solubility / M	Log_{10} P_{ow}
[**2a**]$^+$	$2.3\cdot10^{-3}$	– 1.07 ± 0.08
[**2a^{Fe}**]$^+$ [b]	$3.2\cdot10^{-3}$	– 0.99 ± 0.06 [c]
[**2b**]$^+$	$7.8\cdot10^{-4}$	0.06 ± 0.01
[**2b^{Fe}**]$^+$ [b]	$6.2\cdot10^{-3}$	0.0 ± 0.1
[**2c**]$^+$	$1.6\cdot10^{-3}$	0.05 ± 0.03
[**2c^{Fe}**]$^+$ [b]	$1.4\cdot10^{-3}$	– 0.27 ± 0.04
[**2d**]$^+$	≈ $2\cdot10^{-4}$ [d]	0.10 ± 0.02
[**2d^{Fe}**]$^+$ [b]	≈ $3\cdot10^{-4}$	– 0.46 ± 0.02
[**2e**]$^+$	≈ $1\cdot10^{-4}$ [d]	0.74 ± 0.03
[**2e^{Fe}**]$^+$ [b]	< $3\cdot10^{-4}$	0.29 ± 0.03
[**2h**]$^+$	$1.1\cdot10^{-3}$	0.11 ± 0.03
[**2h^{Fe}**]$^+$ [b]	$2.9\cdot10^{-3}$	– 0.51 ± 0.02

[a] All complexes as $CF_3SO_3^-$ salts. [b] Diiron homologue of the respective diruthenium complex. Data taken from the literature.[4,8] [c] Re-determined with respect to the literature value (– 0.9 ± 0.1). [d] Below the lowest quantitation value ($3\cdot10^{-4}$ M).

Figure S27. ^{1}H NMR spectrum (401 MHz) of a saturated D_2O solution of [**2a**]CF_3SO_3.

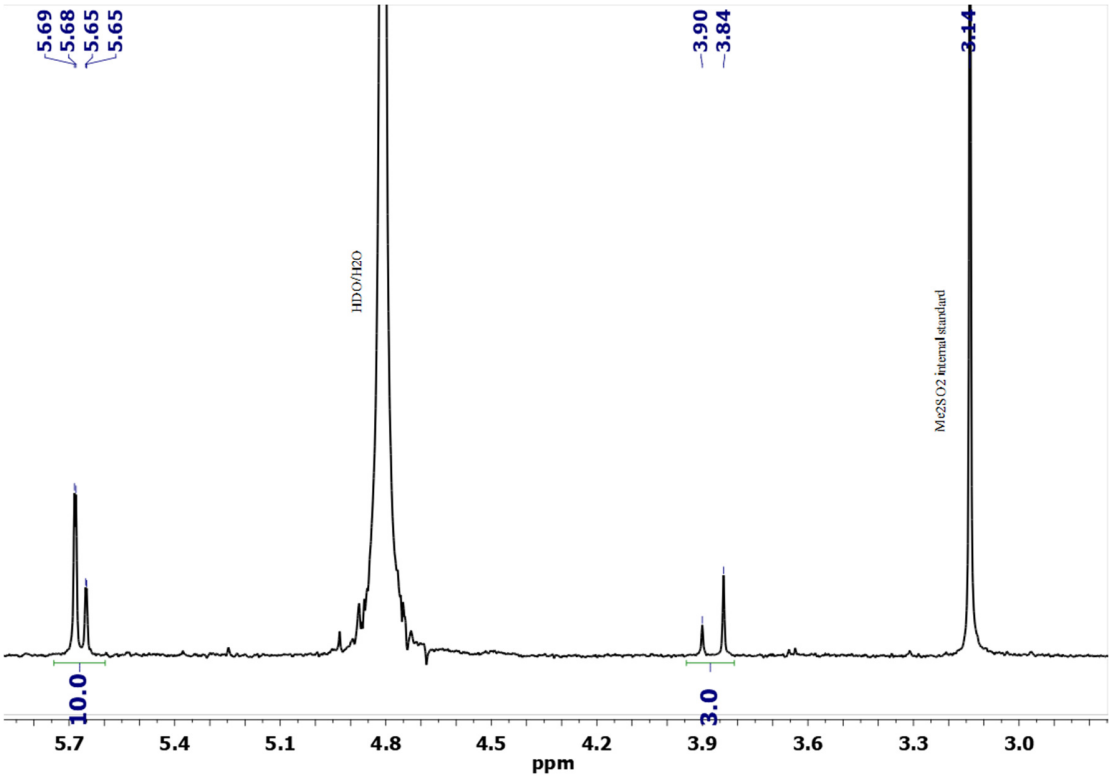

Figure S28. ^{1}H NMR spectrum (401 MHz) of a saturated D_2O solution of [**2b**]CF_3SO_3 (3-6 ppm range).

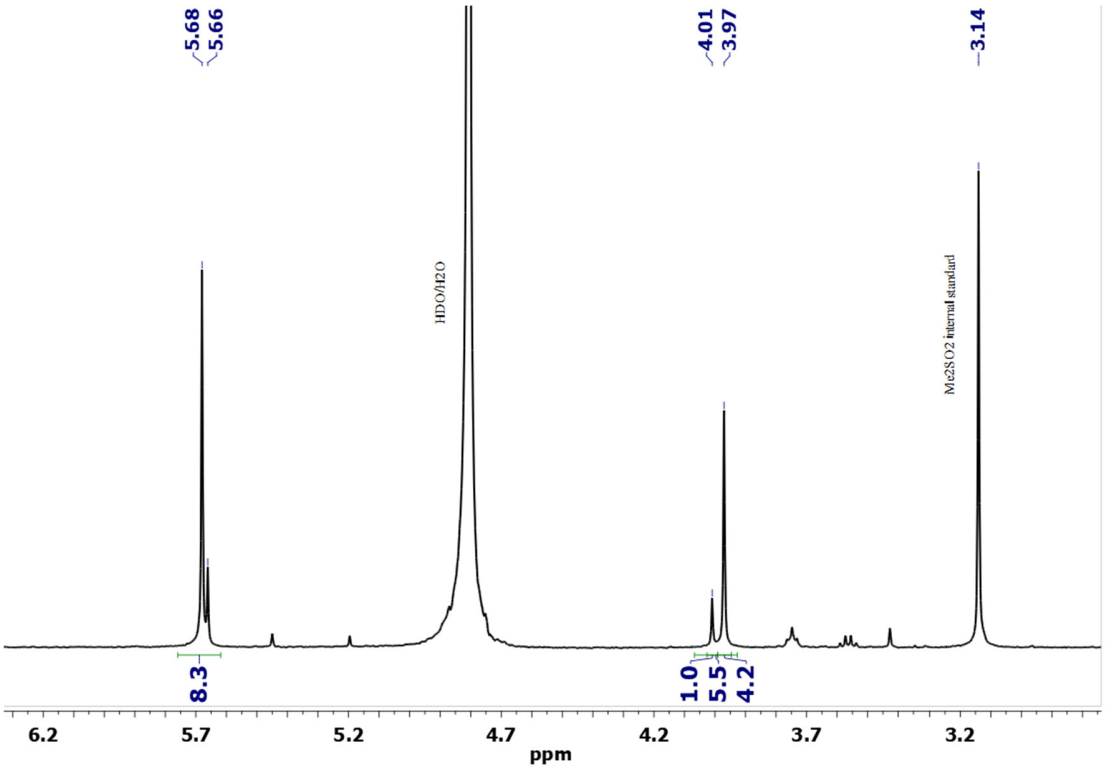

Figure S29. ^{1}H NMR spectrum (401 MHz) of a saturated D_2O solution of [**2c**]CF_3SO_3.

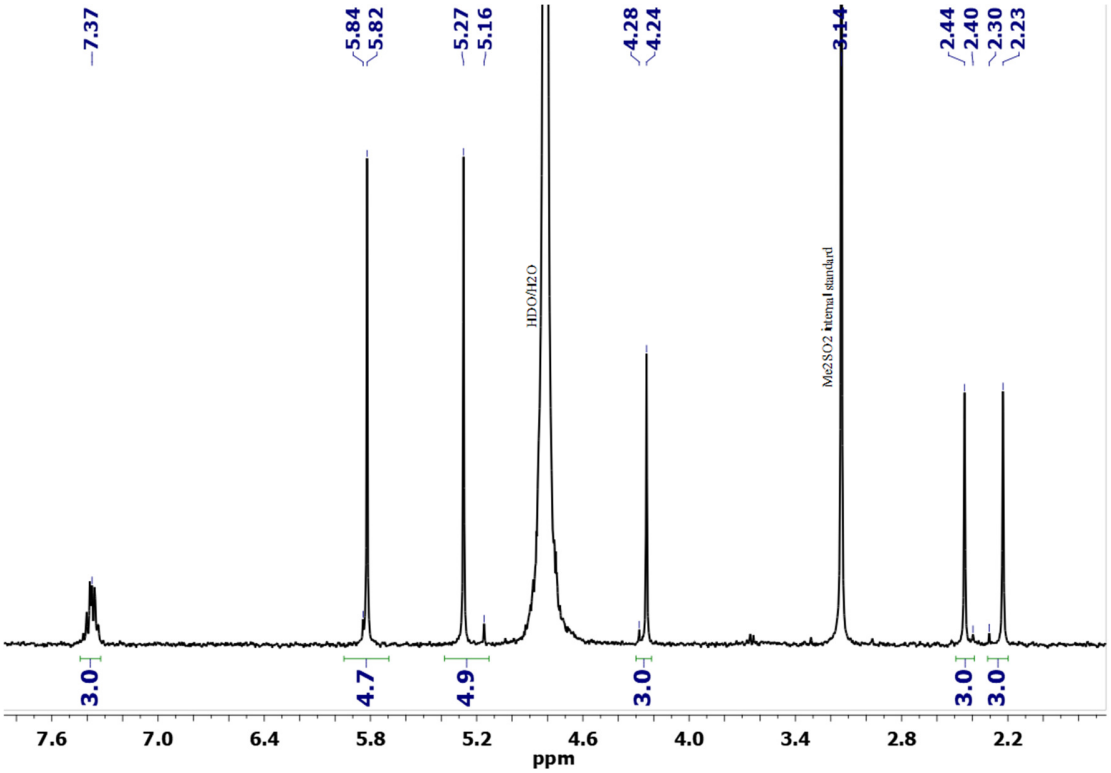

Figure S30. ^{1}H NMR spectrum (401 MHz) of a freshly-prepared solution of [**2c**]CF_3SO_3 in D_2O/CD_3OD 5:3 *v*/*v* (top, cyan line) and after 72 h at 37 °C (bottom, red line).

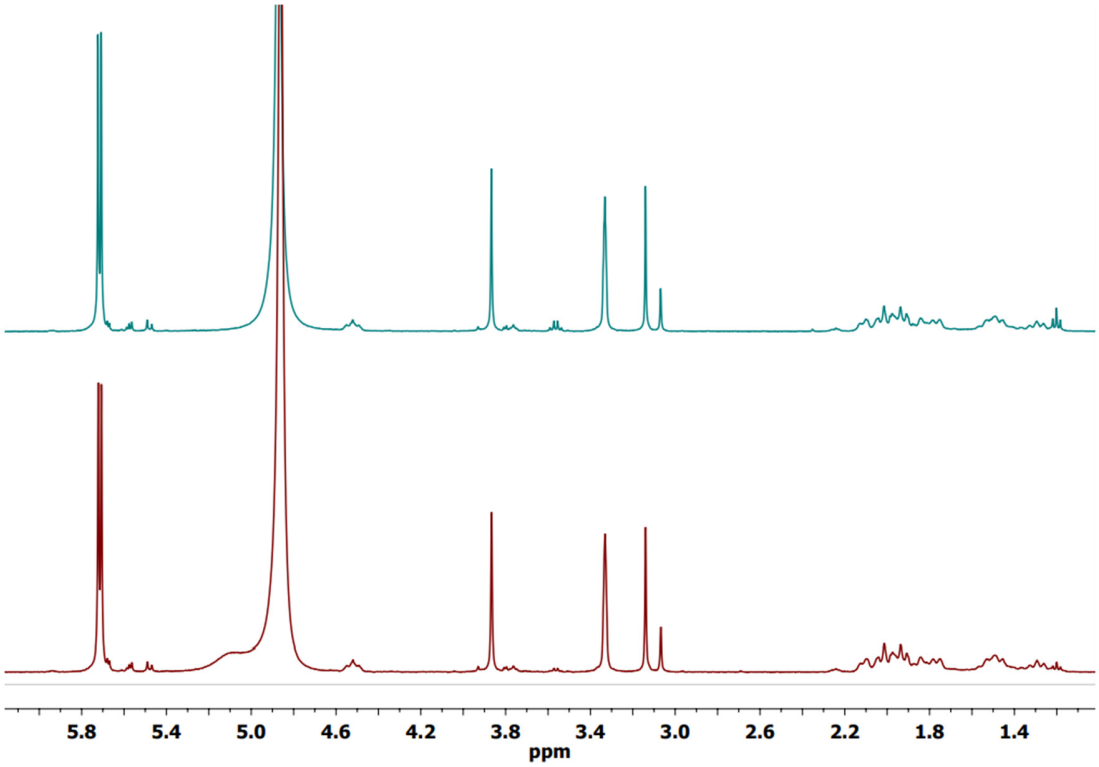

NMR data for D_2O and D_2O/CD_3OD solutions.

[**2a**]CF_3SO_3. ^{1}H NMR (D_2O): δ/ppm = 5.68, *5.66* (s, 10H); *4.01*, 3.97 (s, 6H). ^{1}H NMR (D_2O/CD_3OD 5:3 *v*/*v*): δ/ppm = 5.71, *5.69* (s, 10H); *4.04,* 4.01 (s, 6H). Isomer (*cis*/*trans*) ratio = 4.5 (D_2O); ≈ 11 (D_2O/CD_3OD 5:3 *v*/*v*).

[**2b**]CF_3SO_3. ^{1}H NMR (D_2O): δ/ppm = 5.69, 5.68, *5.65, 5.65* (s, 10H); *3.90*, 3.84 (s, 3H); 2.12−1.34 (m, 10H). ^{1}H NMR (D_2O/CD_3OD 5:3 v/v): δ/ppm = 5.72, 5.71, *5.68*, *5.67* (s, 10H); 4.57−4.48 (m, 1H); *3.93*, 3.87 (s, 3H); 2.16−1.68, 1.57−1.23 (m, 10H). Isomer (*cis*/*trans*) ratio = 2.5 (D_2O); ≈ 30 (D_2O/CD_3OD 5:3 *v*/*v*).

[**2c**]CF_3SO_3. ^{1}H NMR (D_2O): δ/ppm = 7.44–7.32 (m, 3H), *5.84*, 5.82 (s, 5H); 5.27, *5.16* (s, 5H); *4.28*, 4.24 (s, 3H), 2.44, *2.40* (s, 3H), *2.30*, 2.23 (s, 3H). ^{1}H NMR (D_2O/CD_3OD 5:3 v/v): δ/ppm = 7.48–7.35 (m, 3H); *5.87*, 5.86 (s, 5H); 5.30, *5.17* (s, 5H); *4.30*, 4.26 (s, 3H); 2.47, *2.42* (s, 3H); *2.33*, 2.24 (s, 3H). Isomer (*cis*/*trans*) ratio ≈ 25 (D_2O and D_2O/CD_3OD 5:3 v/v).

[**2d**]CF_3SO_3. ^{1}H NMR (D_2O): δ/ppm = 8.45 (s); 7.81 (d, *J* = 2.0 Hz, 1H); 7.70 (d, *J* = 8.6 Hz, 1H); 7.55 (d, *J* = 3.2 Hz, 1H); 7.34 (dd, *J* = 8.6, 2.0 Hz, 1H); 6.71 (dd, *J* = 3.1, 0.7 Hz, 1H); 5.78 (s, 5H); 5.11, *4.99* (s, 5H); *4.48*, 4.40 (s, 3H). Isomer (*cis*/*trans*) ratio ≈ 11 (D_2O).

[**2e**]CF_3SO_3.* ^{1}H NMR (D_2O): ppm = 8.22 (d, *J* = 8.7 Hz, 1H), 8.15–8.04 (m, 3H), 7.77–7.70 (m, 2H), 7.67 (dd, *J* = 8.7, 1.9 Hz, 1H), 5.84 (s, 5H), 5.12 (s, 5H), 4.46 (s, 3H). The presence of {RuCp} by-products in the isolated material prevented unambiguous identification of the ^{1}H NMR set of signals of the *trans* isomer.

[**2h**]CF_3SO_3. ^{1}H NMR (D_2O): /ppm = 7.59–7.35 (m, 5H), 5.75 (s, 5H), 5.64 (s, 5H), 5.59–5.49 (m, 2H), 3.88 (s, 3H). ^{1}H NMR (D_2O/CD_3OD 5:3 v/v): δ/ppm = 7.58–7.29 (m, 5H), 5.78 (s, 5H), 5.68 (s, 5H), 5.62–5.54 (m, 2H), 3.90 (s, 3H). The presence of {RuCp} by-products in the isolated material prevented unambiguous identification of the ^{1}H NMR set of signals of the *trans* isomer.

Cyclic voltammograms in CH_2Cl_2 solution

Figure S31. Cyclic voltammetries of [**2b**]CF_3SO_3 in a 1.0 mM CH_2Cl_2 solution recorded at a Pt electrode between –1.8 and +1.9 V (blue line), and between –1.5 and +1.8 V (red line). $[N^nBu_4]PF_6$ (0.2 mol·dm^{-3}) as supporting electrolyte. Scan rate: 0.1 V s^{-1}. Arrow indicates scan direction.

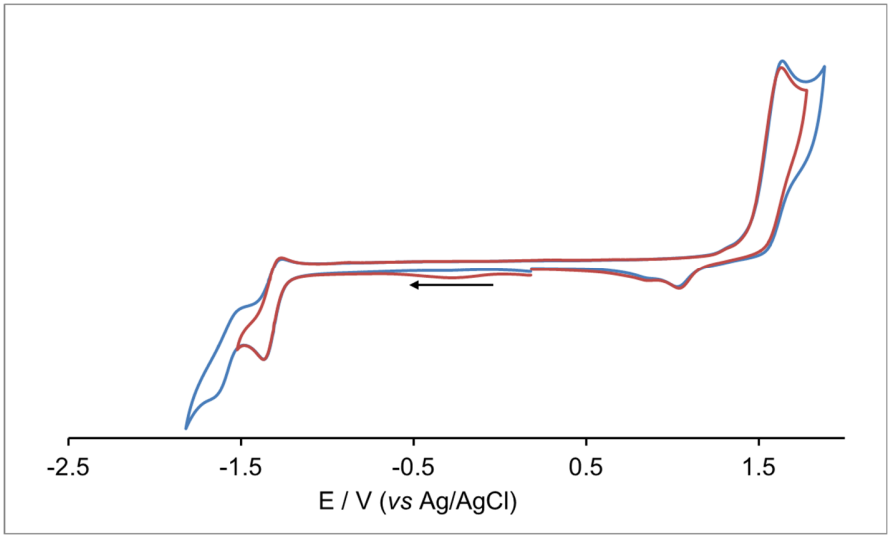

Figure S32. Cyclic voltammetries of [**2c**]CF_3SO_3 in a 1.0 mM CH_2Cl_2 solution recorded at a Pt electrode between +1.8 and –2.1 V (blue line), and between +1.8 and -1.55 V (red line). $[N^nBu_4]PF_6$ (0.2 mol·dm^{-3}) as supporting electrolyte. Scan rate: 0.1 V s^{-1}. Arrow indicates scan direction.

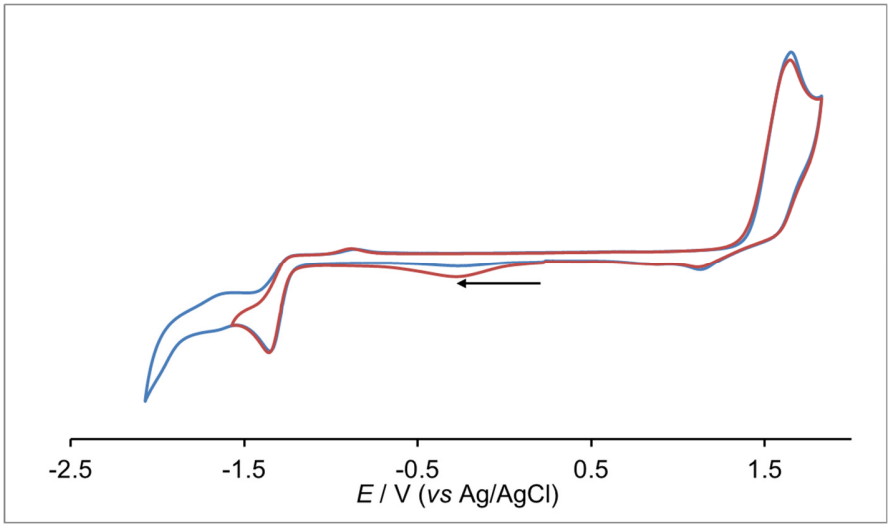

X-Ray crystallography

Table S4. Crystal data and measurement details for [**2a-c**]CF_3SO_3.

	[**2a**]CF_3SO_3	[**2b**]CF_3SO_3	[**2c**]CF_3SO_3
Formula	$C_{17}H_{16}F_3NO_6Ru_2S$	$C_{22}H_{24}F_3NO_6Ru_2S$	$C_{24}H_{22}F_3NO_6Ru_2S$
FW	621.51	689.63	711.62
T, K	100(2)	100(2)	100(2)
λ, Å	0.71073	0.71073	0.71073
Crystal system	Triclinic	Monoclinic	Triclinic
Space group	$P\bar{1}$	$P2_1/n$	$P\bar{1}$
a, Å	8.9719(4)	9.0966(5)	10.0364(4)
b, Å	10.3691(5)	17.9290(10)	10.2272(4)
c, Å	11.3983(5)	14.9387(9)	12.5765(5)
α,°	92.9110(10)	90	95.5780(10)
β,°	104.6700(10)	101.888(2)	97.7480(10)
γ,°	96.868(2)	90	100.7070(10)
Cell Volume, Å^3	1014.83(8)	2384.1(2)	1246.90(9)
Z	2	4	2
D_c, g·cm^{-3}	2.034	1.921	1.895
μ, mm^{-1}	1.653	1.418	1.359
F(000)	608	1368	704
Crystal size, mm	0.16×0.14×0.12	0.24×0.20×0.16	0.22×0.18×0.14
θ limits,°	1.853–25.996	1.797–26.999	2.043–27.993
Reflections collected	13509	50560	21088
Independent reflections	3970 [R_{int} = 0.0283]	5208 [R_{int} = 0.0382]	6014 [R_{int} = 0.0180]
Data / restraints /parameters	3970 / 301 / 346	5208 / 0 / 317	6014 / 0 / 337
Goodness on fit on F^2	1.097	1.151	1.127
R_1 (I > 2σ(I))	0.0220	0.0179	0.0177
wR_2 (all data)	0.0532	0.0420	0.0411
Largest diff. peak and hole, e Å^{-3}	0.495 / –0.870	0.313 / –0.404	0.524 / –0.463

Table S5. Crystal data and measurement details for [**2d,g**]CF_3SO_3.

	[**2d**]CF_3SO_3	[**2g**]CF_3SO_3
Formula	$C_{24}H_{19}F_3N_2O_6Ru_2S$	$C_{24}H_{22}F_3NO_6Ru_2S$
FW	722.61	711.62
T, K	100(2)	100(2)
λ, Å	0.71073	0.71073
Crystal system	Monoclinic	Triclinic
Space group	$P2_1/c$	$P\bar{1}$
a, Å	9.2614(8)	9.195(5)
b, Å	20.816(4)	10.654(7)
c, Å	12.842(2)	13.106(7)
α,°	90	103.45(4)
β,°	98.530(5)	90.26(5)
γ,°	90	91.24(4)
Cell Volume, Å^3	2448.3(8)	1248.4(12)
Z	4	2
D_c, g·cm^{-3}	1.960	1.893
μ, mm^{-1}	1.387	1.357
F(000)	1424	704
Crystal size, mm	0.15×0.11×0.06	0.15×0.13×0.10
θ limits,°	1.878–22.994	1.966–27.000
Reflections collected	16763	18111
Independent reflections	3347 [R_{int} = 0.1183]	10701 [R_{int} = 0.0538]
Data / restraints /parameters	3347 / 228 / 334	10701 / 21 / 672
Goodness on fit on F^2	1.242	1.084
R_1 ($I > 2\sigma(I)$)	0.1457	0.0424
wR_2 (all data)	0.3228	0.1082
Largest diff. peak and hole, e Å^{-3}	2.893 / –2.922	2.401 / –1.564

Figure S33. Comparative view of LC-MS spectra: **A**) [**2a**]CF_3SO_3 in methanol solution; **B**) [**2a**]CF_3SO^3 (10 μM) in admixture with GSH (10 μM) in methanol/water solution after 24h incubation. Specific peaks corresponding to GSH and [**2a**]$^+$ are highlighted with green and blue rectangles, respectively.

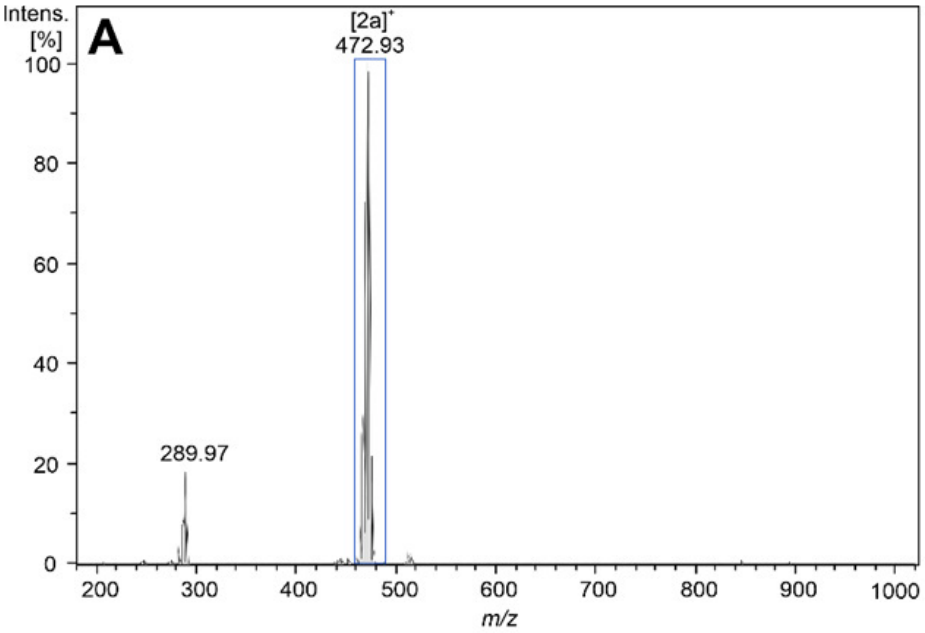

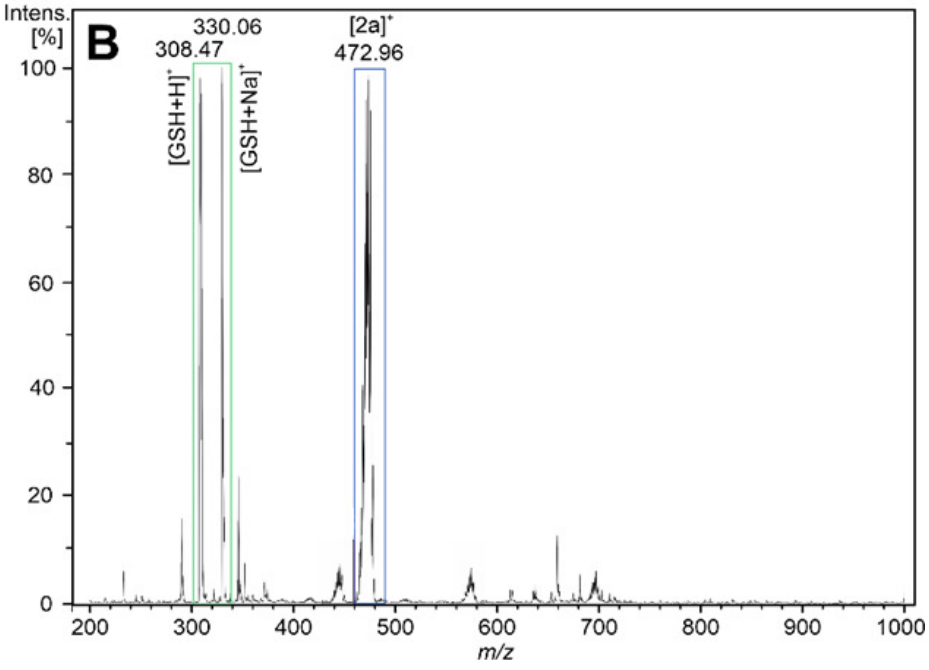

Figure S34. Comparative view of LC-MS spectra: **A**) [**2d**]CF_3SO_3 in methanol solution; **B**) [**2d**]CF_3SO^3 (10 μM) in admixture with GSH (10 μM) in methanol/water solution after 24h incubation. Specific peaks corresponding to GSH and [**2d**]$^+$ are highlighted with green and blue rectangles, respectively.

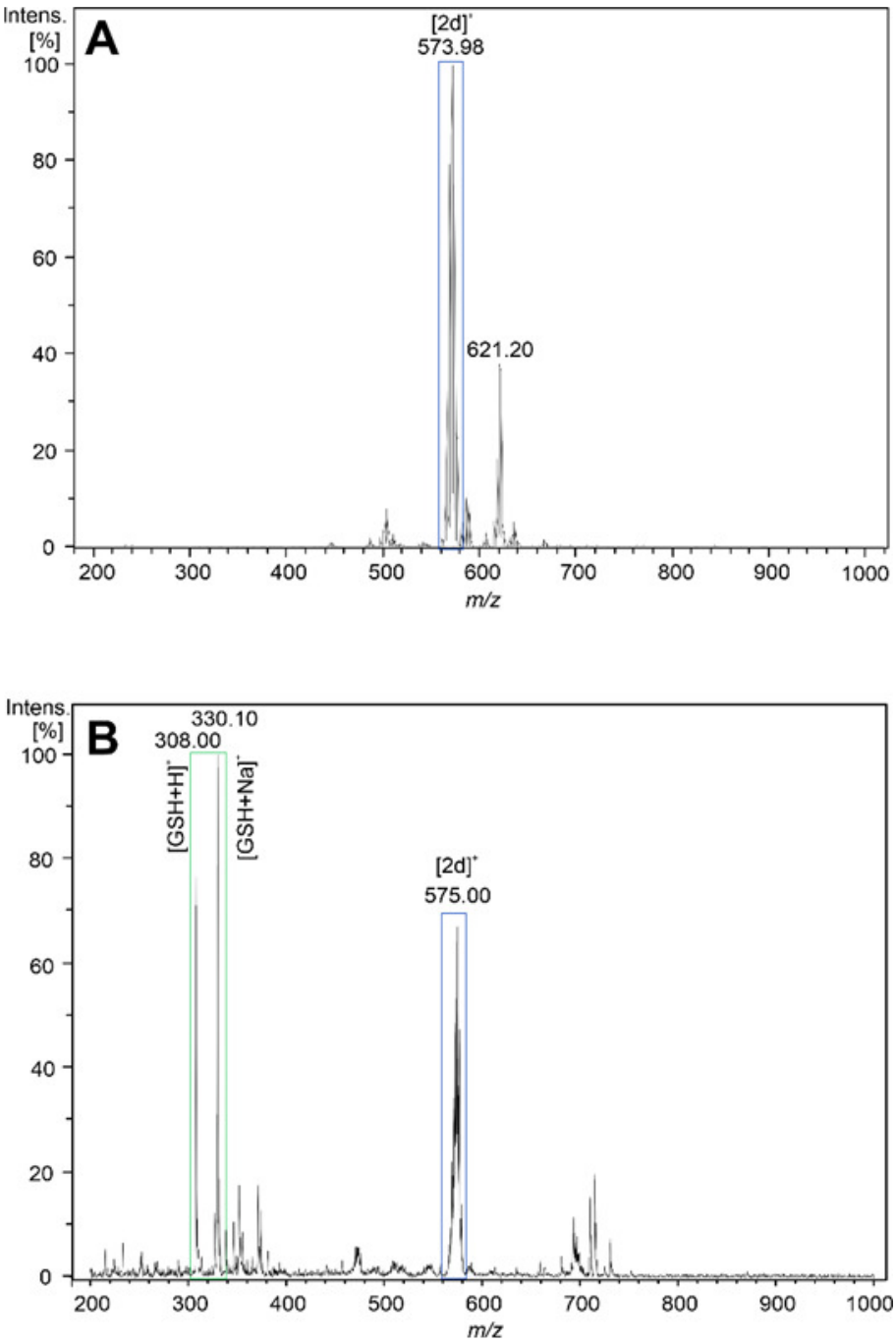

Figure S35. MALDI-TOF MS spectra of native bovine serum albumin (BSA, top panel), and mixtures of BSA with [**2a**]CF_3SO_3 (middle panel), and [**2d**]CF_3SO_3 (bottom panel) after 48h incubation, suggesting no significant formation of covalent or non-covalent adducts. The indicated values represent the average mass determined from six independent measurements ± the standard deviation.

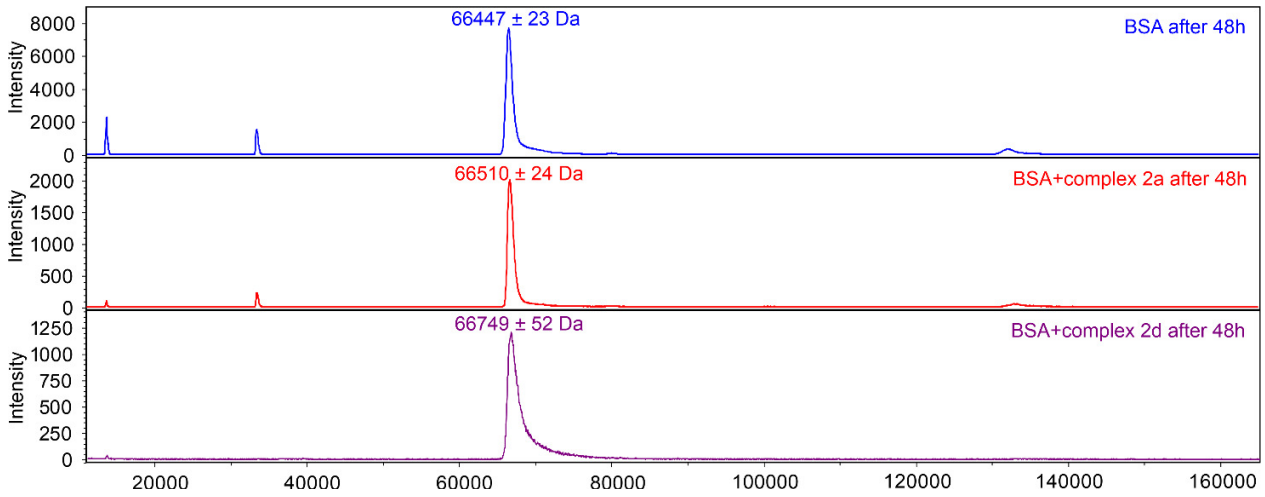

References

1 J. Yin, J. Zhang, C. Cai, G.-J. Deng, H. Gong, Catalyst-Free Transamidation of Aromatic Amines with Formamide Derivatives and Tertiary Amides with Aliphatic Amines, *Org. Lett.* 2019, **21**, 387−392.

2 M. A. Mironov, M. I. Tokareva, M. N. Ivantsova, V. S. Mokrushin, Ugi Reaction with Isocyanoindoles, Russ. *J. Org. Chem.* 2004, **40**, 847–853.

3 N. M. Doherty, S. A. R. Knox, M. J. Morris, C. P. Casey, G. T. Whiteker, Tetracarbonylbis(h5-cyclopentadienyl)diruthenium, *Inorg. Synth.* 1990, 189-191.

4 L. Biancalana, M. De Franco, G. Ciancaleoni, S. Zacchini, G. Pampaloni, V. Gandin, F. Marchetti, Easily Available and Amphiphilic Diiron Cyclopentadienyl Complexes Exhibit In Vitro Anticancer Activity in 2D and 3D Human Cancer Cells via Redox Modulation Triggered by CO Release, *Chem. Eur. J.* 2021, **27**, 10169–10185.

5 L. Biancalana, M. Kubeil, S. Schoch, S. Zacchini, F. Marchetti, Switching on Cytotoxicity of Water-Soluble Diiron Organometallics by UV Irradiation, *Inorg. Chem.* 2022, **61**, 7897–7909.

6 G. Agonigi, M. Bortoluzzi, F. Marchetti, G. Pampaloni, S. Zacchini, V. Zanotti, Regioselective Nucleophilic Additions to Diiron Carbonyl Complexes Containing a Bridging Aminocarbyne Ligand: A Synthetic, Crystallographic and DFT Study, *Eur. J. Inorg. Chem.* 2018, 960–971.

7 G. Albano, L. Busetto, M. Monari, V. Zanotti, Reactions of acetonitrile di-iron m-aminocarbyne complexes; synthesis and structure of [Fe2(μ-CNMe2)(m-H)(CO)2(Cp)2], *J. Organomet. Chem*. **606**, 2000, 163-168.

8 G. Agonigi, L. Biancalana, M. G. Lupo, M. Montopoli, N. Ferri, S. Zacchini, F. Binacchi, T. Biver, B. Campanella, G. Pampaloni, V. Zanotti and F. Marchetti, Exploring the Anticancer Potential of Diiron Bis-cyclopentadienyl Complexes with Bridging Hydrocarbyl Ligands: Behavior in Aqueous Media and In Vitro Cytotoxicity, *Organometallics* 2020, **39**, 645-657.